Fixed-Time Generalized Active Disturbance Rejection With Quasi-Resonant Control for PMSM Speed Disturbances Suppression

Xiufeng Liu, *Graduate Student Member, IEEE*, Yongting Deng, *Senior Member, IEEE*, Jianli Wang, *Member, IEEE*, Hongwen Li, *Member, IEEE*, and Haiyang Cao, *Graduate Student Member, IEEE*

***Abstract*—Robust and smooth speed control is very important for permanent magnet synchronous motor (PMSM) drives. However, aperiodic and periodic disturbances generally exist in PMSM system, which affects the stability of the system and causes speed fluctuations. Therefore, this article proposes a fixed-time switching generalized active disturbance rejection control method with a switching quasi-resonant controller to achieve satisfactory speed control performance. First, a fixed-time switching generalized extended state observer whose state estimation errors can converge to steady state in a fixed time is used to suppress the aperiodic disturbances. Second, a switching quasi-resonant controller that can avoid the side effect of resonant terms during motor dynamics is designed to attenuate the speed fluctuations caused by the periodic disturbances. Then, the performance of the proposed scheme is systematically analyzed. Finally, the feasibility and effectiveness of the proposed method are verified on a 5.5-kW PMSM experimental platform.**

***Index Terms*—Fixed-time control theory, generalized active disturbance rejection control (GADRC), permanent magnet synchronous motor (PMSM), quasi-resonant controller (QRC).**

I. Introduction

PERMANENT magnet synchronous motor (PMSM) has been extensively employed in high-precision servo systems owing to its superior torque inertia ratio, high power density, and high reliability, such as electric vehicles, robots, large-scale telescopes, and various other fields [1], [2], [3]. However, there exist aperiodic and periodic disturbances in PMSM drive system, which will cause speed fluctuations and reduce the speed control performance. The aperiodic disturbances mainly include external load torque and model parameters uncertainty, while the periodic disturbances mainly include flux harmonics, inverter nonlinearity, current sampling errors, and cogging torque. Therefore, to achieve robust and smooth speed control, many different disturbance suppression schemes have been investigated in recent years.

Over the past few years, the effective methods for suppressing the aperiodic disturbances include active disturbance rejection control (ADRC) [4], [5], [6], adaptive control [7], model predictive control [8], sliding mode control [9], [10], extended Kalman filter (EKF) [11], [12], intelligent control [13], etc. Among these methods, ADRC is receiving increasing attention as it is relatively less reliant on the model information [14]. As the core of ADRC, extended state observer (ESO) can estimate all the aperiodic disturbances as lumped disturbance and compensate it to the feedback control law to suppress the aperiodic speed fluctuations. However, the conventional linear ESO (CLESO) has the limited ability to observe the fast-varying disturbance, and the estimation error of the CLESO for fast-varying disturbance cannot converge asymptotically [3], [15]. To overcome this problem, the linear generalized ESO (LGESO), also known as the generalized proportional integral observer, has been proposed [16], which has a higher estimation accuracy to the fast-varying disturbances by increasing the order of the observer.

Meanwhile, the CLESO can only asymptotically converge in an infinite domain. Therefore, to improve the convergence rate of the CLESO, the fixed-time ESOs (FESOs) based on the fixed-time control theory [17], [18] have been studied by more and more researchers in [19], [20], [21], [22], and [23], whose convergence time is bounded by a fixed constant independent of the initial conditions. Owing to this attractive characteristic, FESOs have been successfully employed in a range of academic and practical applications, such as robotic systems, spacecraft, and multiagent systems with second-order dynamics [19], [20], [21]. However, the correction terms of these FESOs contain sign functions, which will cause high-frequency chattering. To solve this problem, the fixed-time GESO (FGESO) with continuous correction terms has been proposed in [22] and [23]. Although the abovementioned FGESO avoids the high-frequency chattering problem caused by the sign functions, the nonlinear

Manuscript received 24 July 2023; revised 16 November 2023 and 30 January 2024; accepted 11 March 2024. Date of publication 14 March 2024; date of current version 19 April 2024. This work was supported in part by the National Natural Science Foundation of China under Grant 11973041 and Grant 12122304, in part by the Jilin Province Key R&D Plan Project under Grant 20220203036SF, and in part by the Jilin Province Science and Technology Innovation Platform Project under Grant 20230505007ZP. Recommended for publication by Associate Editor H. Hofmann. *(Corresponding author: Yongting Deng.)*

Xiufeng Liu, Jianli Wang, and Haiyang Cao are with the Changchun Institute of Optics, Fine Mechanics, and Physics, Chinese Academy of Science, Changchun 130033, China, and also with the University of Chinese Academy of Sciences, Beijing 100049, China (e-mail: liuxiufeng20@mails.ucas.ac.cn; wangjianli@ciomp.ac.cn; caohaiyang20@mails.ucas.ac.cn).

Yongting Deng and Hongwen Li are with the Changchun Institute of Optics, Fine Mechanics, and Physics, Chinese Academy of Science, Changchun 130033, China (e-mail: dengyongting@ciomp.ac.cn; lihongwen@ciomp.ac.cn).

Color versions of one or more figures in this article are available at https://doi.org/10.1109/TPEL.2024.3377186.

Digital Object Identifier 10.1109/TPEL.2024.3377186

TABLE I
COMPARISON OF THE EXISTING ESOS

Methods	Aperiodic disturbance suppression	Fast-varying disturbance suppression	Convergence time	Sensitivity to high-frequency disturbance and noise
CLESO	√	poor	infinite domain	insensitive
LGESO	√	good	infinite domain	insensitive
FESO	√	poor	fixed time	sensitive
FGESO	√	good	fixed time	sensitive
LNSESO	√	poor	\	insensitive

FGESO still has the chattering caused by high-frequency disturbance and noise, which results in a large limitation on the observer performance and practical application. In [24], [25], and [26], linear/nonlinear switching ESOs (LNSESOs) have been proposed to reduce the sensitivity of the ESO to high-frequency disturbance and noise, which integrate the advantages of the C-LESO and nonlinear ESO. Table I further shows the strengths and weaknesses of the abovementioned methods. From Table I, it can be seen that the existing ESOs all have some flaws. Therefore, using the linear/nonlinear switching control strategy, a fixed-time switching GESO (FSGESO) is proposed for PMSM drive system to suppress the aperiodic disturbances in this article, which integrates the merits of the FGESO and LGESO, not only can converge to steady state in a fixed time but also can reduce the sensitivity of the observer to system high-frequency disturbance and noise.

Although the proposed FSGESO algorithm is proficient in estimating aperiodic disturbances, it demonstrates inadequate performance in suppressing periodic disturbances. Consequently, the integration of an auxiliary component into the proposed FSGESO is essential to effectively deal with the periodic disturbances. Recently, several auxiliary components, such as iterative learning controller [27], repetitive controller [28], and resonant controller [29], [30], [31], have been proposed in combination with ADRC to suppress periodic disturbances. Among these methods, resonant controller is particularly popular for its ability to suppress periodic disturbances. Wang has added a conventional quasi-resonant controller (CQRC) to the linear ADRC for PMSM speed regulation to suppress the aperiodic and periodic disturbances in [29]. Tian et al. [30] proposed an adaptive linear ADRC with an adaptive resonant controller which can estimate the uncertain periodic disturbances for PMSM current disturbances suppression. Although, those methods can effectively attenuate the periodic disturbances, the side effect of resonant terms during motor dynamics is not considered. To solve this problem, Xia et al. [31] proposed a proportional-integral-resonant (PIR) controller by switching resonant mode to avoid transient instability and obtain high-precision speed control performance. However, the limited gain bandwidth of the PIR could negatively impact the stability of the system. Hence, a switching quasi-resonant controller (SQRC) designed by the switching resonant mode will be an effective and practical method for suppressing periodic disturbances.

Motivated by the abovementioned investigations, to obtain robust and smooth speed control, this article proposes an FSGESO with an SQRC for PMSM drive system to attenuate the aperiodic and periodic disturbances. The main contributions of this article are summarized as follows.

1) An FSGESO is proposed for PMSM speed control to suppress the aperiodic disturbances, which possesses the advantages of the FGESO and LGESO. The FSGESO not only can converge to steady state in a fixed time but also can reduce the sensitivity to the system high-frequency disturbance and noise. In addition, the performance limitation of the FGESO existing in [22] and [23] is mitigated by using the linear/nonlinear switching control strategy.
2) An SQRC is designed to enhance the control law to attenuate the periodic disturbances, which is implemented in parallel with the FSGESO. The SQRC avoids the transient instability through the automatic switching resonant mode, and its gain bandwidth can be adjusted by its cut-off frequency.
3) The proposed FSGESO-SQRC method can effectively eliminate the aperiodic and periodic disturbances to achieve robust and smooth speed control performance.

The rest of this article is organized as follows. Section II introduces the mathematical mode of PMSM and analyzes the disturbances in PMSM. The proposed FSGESO-SQRC is designed in Section III. Performance Analysis of the system with the proposed FSGESO-SQRC is given in Section IV. In Section V, experiments are carried out to verify the proposed scheme. Finally, Section VI concludes this article.

II. MATHEMATICAL MODELS AND DISTURBANCES ANALYSIS

A. Mathematical Model of PMSM

Neglecting the effects of hysteresis loss, core saturation and eddy current of the surface-mounted PMSM, the dq-axis voltage equation in the synchronous rotating reference frame is expressed as [1]

$$\begin{cases} u_d = R_s i_d + L_d \frac{di_d}{dt} - \omega_m n_p L_q i_q \\ u_q = R_s i_q + L_q \frac{di_q}{dt} + \omega_m n_p (L_d i_d + \psi_f) \end{cases} \tag{1}$$

where u_d and u_q are the d- and q-axis stator voltages, $L_d = L_q = L_s$ are the d- and q-axis stator inductance, i_d and i_q are the d- and q-axis stator currents, respectively. R_s is the stator resistance, ω_m is the rotor mechanical angular speed, n_p is the number of pole pairs, and ψ_f is the permanent magnet flux linkage.

The dynamic equation of PMSM can be expressed as

$$J\dot{\omega}_m = T_e - B\omega_m - T_L \tag{2}$$

where T_e is the electromagnetic torque, B is the viscous frictional coefficient, J is the inertia, and T_L is the load torque.

By utilizing the field-oriented control strategy, we can get the maximize output torque when the d-axis current is zero ($i_d = 0$). Then, the electromagnetic torque equation can be presented as

$$T_e = \frac{3}{2} n_p i_q [i_d (L_d - L_q) + \psi_f] = \frac{3}{2} n_p \psi_f i_q = K_t i_q \tag{3}$$

where K_t is the torque coefficient.

B. Disturbances Analysis

The aperiodic disturbances in PMSM mainly include external load torque and model parameters uncertainty. Considering the change of model parameters, the dynamic equation (2) of PMSM can be expressed as

$$(J_0+\Delta J)\dot{\omega}_m=(K_{t0}+\Delta K_t)i_q-(B_0+\Delta B)\omega_m-T_L \tag{4}$$

where J_0, K_{t0}, and B_0 are the rated values of inertia, torque coefficient, and viscous friction coefficient, $\Delta J=J-J_0$, $\Delta K_t=K_t-K_{t0}$, and $\Delta B=B-B_0$ are the mismatch values of the inertia, torque coefficient, and viscous friction coefficient, respectively.

The periodic disturbances that exist in PMSM drive system mainly include flux harmonics, inverter nonlinearity, current measurement errors, and cogging torque. According to the literature [1], the periodic disturbances will cause torque ripples, thereby the speed fluctuations will be induced by the torque ripples. Considering the abovementioned periodic disturbances, the total torque harmonics caused by the periodic disturbances can be expressed as

$$\begin{aligned}T_h&=f(\psi_h,u_{dh},u_{qh},T_{\text{cog}},T_{\text{offset}},T_{\text{scaling}})\\&=T_1\cos(\theta_e+\theta_1)+T_2\cos(2\theta_e+\theta_2)\\&\quad+\sum_{n=1}^{\infty}T_{6n}\cos(6n\theta_e+\theta_{6n})+\sum_{n=1}^{\infty}T_{\text{cog}}^{n}\sin(nN_c\theta_e)\end{aligned} \tag{5}$$

where ψ_h is the flux harmonics, u_{dh} and u_{qh} are the voltage harmonics caused by the inverter nonlinearity, T_{cog} is the cogging torque, T_{offset} and T_{scaling} are the torque harmonics caused by the current offset error and scaling error, T_1, T_2, and T_{6n} are the amplitudes of the first, second, and $6n$th torque harmonics, θ_1, θ_2, and θ_{6n} are the phase angle of the first, second, and $6n$th torque harmonics, respectively, T_{cog}^{n} is the magnitude of the nN_cth cogging torque harmonics, and N_c is the least common multiple of the number of motor cogging and pole pairs.

Based on the abovementioned analysis, under the aperiodic and periodic disturbances, the dynamic equation of PMSM can be expressed as

$$(J_0+\Delta J)\dot{\omega}_m=(K_{t0}+\Delta K_t)i_q-(B_0+\Delta B)\omega_m-T_L+T_h. \tag{6}$$

Furthermore, the PMSM dynamic equation (6) can be represented as the following disturbed system:

$$\begin{cases}\dot{x}_1=d+b_0u\\ y=x_1\end{cases} \tag{7}$$

where $x_1=\omega_m$ is the system state, $u=i_{q,\text{ref}}$ is the control input, $y=\omega_m$ is the system output, $b_0=K_{t0}/J_0$, and $d=(\Delta K_t i_q-B\omega_m-T_L+T_h-\Delta J\dot{\omega}_m)/J_0$ is the lumped disturbance.

III. Design of the Proposed FSGESO-SQRC

In order to suppress the aperiodic and periodic disturbances exist in PMSM system, this section proposes an FSGESO-SQRC method. First, an FSGESO is proposed and its fixed-time convergence property is proved systematically. Then, an SQRC is designed in parallel with the FSGESO. Finally, the structure diagram of the FOC-based PMSM with the proposed FSGESO-SQRC is shown.

A. Design of the FSGESO

First, system (7) can be extended as

$$\begin{cases}\dot{\mathbf{x}}=\mathbf{A}\mathbf{x}+\mathbf{B_0}u+\mathbf{D}d^{(n-1)}\\ y=\mathbf{C}\mathbf{x}\end{cases} \tag{8}$$

where $\mathbf{x}=[x_1\ \ x_2\ \ x_3\ \ \cdots\ \ x_n]^T=[\omega_m\ \ d\ \ \dot{d}\ \ \cdots\ \ d^{(n-2)}]^T$, $\mathbf{A}=\begin{bmatrix}0&1&0&\cdots&0\\0&0&1&\ddots&\vdots\\\vdots&\vdots&\ddots&\ddots&0\\0&0&\cdots&0&1\\0&0&\cdots&0&0\end{bmatrix}$, $\mathbf{B_0}=\begin{bmatrix}b_0\\0\\0\\\vdots\\0\end{bmatrix}$, $\mathbf{D}=\begin{bmatrix}0\\0\\\vdots\\0\\1\end{bmatrix}$, $\mathbf{C}=\begin{bmatrix}1\\0\\0\\\vdots\\0\end{bmatrix}^T$.

Assumption 1: The $(n-1)$th derivative of the disturbance $d^{(n-1)}$ exists and satisfies $|d^{(n-1)}|\leqslant d_{\max}^{(n-1)}$, where $d_{\max}^{(n-1)}$ denotes the upper bound.

Then, the FSGESO of system (8) can be designed as

$$\begin{cases}\dot{\hat{x}}_1=\hat{x}_2+b_0u+k_1\omega_0\psi(\delta,\vartheta_1,\gamma_1,\hat{e}_1)\\ \dot{\hat{x}}_2=\hat{x}_3+k_2\omega_0^2\psi(\delta,\vartheta_2,\gamma_2,\hat{e}_1)\\ \dot{\hat{x}}_3=\hat{x}_4+k_3\omega_0^3\psi(\delta,\vartheta_3,\gamma_3,\hat{e}_1)\\ \quad\vdots\\ \dot{\hat{x}}_n=k_n\omega_0^n\psi(\delta,\vartheta_n,\gamma_n,\hat{e}_1)\end{cases} \tag{9}$$

$$\psi(\delta,\vartheta_i,\gamma_i,\hat{e}_1)=\begin{cases}\hat{e}_1/\delta^{1-\vartheta_i}0\leqslant|\hat{e}_1|<\delta\\ \text{sgn}^{\vartheta_i}(\hat{e}_1),\delta\leqslant|\hat{e}_1|\leqslant 1\\ \text{sgn}^{\gamma_i}(\hat{e}_1),|\hat{e}_1|>1\\ i=1,2,\ldots,n\end{cases} \tag{10}$$

where $\hat{\mathbf{x}}=\begin{bmatrix}\hat{x}_1&\hat{x}_2&\cdots&\hat{x}_n\end{bmatrix}^T=\begin{bmatrix}\hat{\omega}_m&\hat{d}&\cdots&\hat{d}^{(n-2)}\end{bmatrix}^T$ is the estimation of $\mathbf{x}$, $\hat{e}_1=x_1-\hat{x}_1$ is the observation error of x_1, $\vartheta_i=i\vartheta-(i-1)$, $\vartheta\in(1-1/n,1)$, $\gamma_i=i\gamma-(i-1)$, $\gamma\in(1,+\infty)(i=1,2,\cdots,n)$, $\omega_0\geqslant 1$ is a constant related to the observer bandwidth, $\delta\in(0,1)$ is the switching point, $\text{sgn}^*(\cdot)\triangleq\text{sign}(\cdot)|\cdot|^*$ where $\text{sign}(\cdot)$ is the sign function, and the observer gain vector $\mathbf{K}=\begin{bmatrix}k_1&k_2&\cdots&k_n\end{bmatrix}^T$ is designed as

$$\mathbf{K}=\mathbf{S^{-1}C^T} \tag{11}$$

where $\mathbf{S}$ is the solution of the Riccati equation [32]

$$\mathbf{S}+\mathbf{A^TS}+\mathbf{SA}-\mathbf{C^TC}=\mathbf{0}. \tag{12}$$

According to (9) and (10), the FSGESO is an FGESO when $|\hat{e}_1|\geq\delta$, while the FSGESO will switch to an LGESO when $|\hat{e}_1|<\delta$. Therefore, taking $|\hat{e}_1|=\delta$ as the switching point, the FSGESO can be divided into the following two cases.

Case 1: When $|\hat{e}_1|\geqslant\delta$, the FSGESO is a nonlinear FGESO. Combining (8) and (9), the differential equation of the estimation error can be expressed as

$$\dot{\hat{\mathbf{e}}}=\mathbf{A}\hat{\mathbf{e}}-\mathbf{\Phi}(\omega_0,\mathbf{K},\vartheta,\gamma,\hat{e}_1)+\mathbf{D}d^{(n-1)} \tag{13}$$

where $\hat{\mathbf{e}} = \begin{bmatrix}\hat{e}_1 & \hat{e}_2 & \cdots & \hat{e}_n\end{bmatrix}^T, \hat{e}_i = x_i - \hat{x}_i (i = 1, 2, \ldots, n)$ is the estimation errors, $\mathbf{\Phi}(\omega_0, \mathbf{K}, \vartheta, \gamma, \hat{e}_1)$ is a vector field with $\Phi_i(\omega_0, k_i, \vartheta_i, \gamma_i, \hat{e}_1) = k_i \omega_o^i \varphi(\vartheta_i, \gamma_i, \hat{e}_1)(i = 1, 2, \ldots, n)$, and where

$$\varphi(\vartheta_i, \gamma_i, \hat{e}_1) = \begin{cases} \operatorname{sgn}^{\vartheta_i}(\hat{e}_1), & 0 \leqslant |\hat{e}_1| \leqslant 1 \\ \operatorname{sgn}^{\gamma_i}(\hat{e}_1), & |\hat{e}_1| > 1. \end{cases} \tag{14}$$

To achieve fixed-time convergence of the observation errors, we introduce a bi-limit homogeneous corrective term $\mathbf{\Phi}(\omega_0, \mathbf{K}, \vartheta, \gamma, \hat{e}_1)$. When $d^{(n-1)} = 0$, the approximation at 0 or at ∞ of (13) is closely related to the behavior of the following standard homogeneous system:

$$\dot{\hat{\mathbf{e}}} = \mathbf{A}\hat{\mathbf{e}} - \mathbf{\Phi}'(\mathbf{K}, \alpha, \hat{e}_1) \tag{15}$$

where $\mathbf{\Phi}'(\mathbf{K}, \alpha, \hat{e}_1)$ is a vector with $\Phi'_i(k_i, \alpha_i, \hat{e}_1) = k_i \operatorname{sgn}^{\alpha_i}(\hat{e}_1)(i = 1, 2, \ldots, n)$, $\alpha_i = i\alpha - (i-1), \alpha \in (1 - 1/n, +\infty)$.

According to Definition 2 given in the Appendix, system (15) is homogeneous of degree $\alpha - 1$ with respect to the weight vector $\mathbf{r}(\alpha) = [r_1 \quad r_2 \quad \cdots \quad r_n]^T$, $r_i = (i-1)\alpha - (i-2)(i = 1, 2, \ldots, n)$. Therefore, we can construct the homogeneous Lyapunov function of system (15) according to the following lemma.

Lemma 1 (see [22]): There exists $\varepsilon > 0$ such that system (15) is asymptotically stable for all $\alpha \in (1 - \varepsilon, 1 + \varepsilon)$. Furthermore, a homogeneous Lyapunov function of degree 2 with respect to the weight vector $\mathbf{r}(\alpha)$, whose 1-level set is exactly the 1-level set $\mathbf{\Xi} \triangleq \{\hat{\mathbf{e}} \in \mathbb{R}^n | \hat{\mathbf{e}}^{\mathbf{T}} \mathbf{S} \hat{\mathbf{e}} = 1\}$ of the quadratic Lyapunov function $V(\hat{\mathbf{e}}) = \hat{\mathbf{e}}^{\mathbf{T}} \mathbf{S} \hat{\mathbf{e}}$, exists and for all $\lambda > 0$ satisfies

$$W_\alpha(\mathbf{\Lambda}_\lambda^{\mathbf{r}(\alpha)} \tilde{\mathbf{z}}) = \lambda^2 W_\alpha(\tilde{\mathbf{z}}) = \lambda^2 V(\tilde{\mathbf{z}}) \tag{16}$$

where $\tilde{\mathbf{z}} \in \mathbf{\Xi}$ and $\mathbf{\Lambda}_\lambda^{\mathbf{r}}$ is defined in the Appendix. Furthermore, the time derivative of the Lyapunov function along the trajectories of system (15) satisfies the following inequality:

$$\dot{W}_\alpha(\hat{\mathbf{e}})|_{(15)} = \left\langle \frac{dW_\alpha(\hat{\mathbf{e}})}{d\hat{\mathbf{e}}}, \mathbf{f}_\alpha(\hat{\mathbf{e}}) \right\rangle \leqslant -\frac{3}{4}(W_\alpha(\hat{\mathbf{e}}))^{\frac{1+\alpha}{2}} \tag{17}$$

where $\mathbf{f}_\alpha(\hat{\mathbf{e}}) = \mathbf{A}\hat{\mathbf{e}} - \mathbf{\Phi}'(\mathbf{K}, \alpha, \hat{e}_1)$.

When $\omega_0 = 1$, the approximations of $\mathbf{\Phi}(\omega_0, \mathbf{K}, \vartheta, \gamma, \hat{e}_1)$ at 0 and at ∞ are $\mathbf{\Phi}'(\mathbf{K}, \vartheta, \hat{e}_1)$ and $\mathbf{\Phi}'(\mathbf{K}, \gamma, \hat{e}_1)$. Then, using the structure of the homogeneous Lyapunov function defined in Lemma 1, we can build two homogeneous Lyapunov functions (one for each approximation): at 0 (resp. ∞) denoted by W_ϑ for $\vartheta < 1$ (resp. W_γ for $\gamma > 1$).

Let us denote two error sets as follows:

$$\begin{aligned} \mathbf{\Xi}_0 &\triangleq \{\mathbf{\Lambda}_\lambda^{\mathbf{r}(\vartheta)} \tilde{z} | \lambda \in (0, 1], \tilde{z} \in \mathbf{\Xi}\} \\ \mathbf{\Xi}_\infty &\triangleq \{\mathbf{\Lambda}_\lambda^{\mathbf{r}(\gamma)} \tilde{z} | \lambda \in [1, \infty), \tilde{z} \in \mathbf{\Xi}\} \end{aligned} \tag{18}$$

which can be equal to

$$\begin{aligned} \mathbf{\Xi}_0 &\triangleq \{\hat{\mathbf{e}} \in \mathbb{R}^n | \hat{\mathbf{e}}^{\mathbf{T}} \mathbf{S} \hat{\mathbf{e}} \leqslant 1\} \\ \mathbf{\Xi}_\infty &\triangleq \{\hat{\mathbf{e}} \in \mathbb{R}^n | \hat{\mathbf{e}}^{\mathbf{T}} \mathbf{S} \hat{\mathbf{e}} \geqslant 1\}. \end{aligned} \tag{19}$$

Then, the candidate homogeneous Lyapunov function is defined as

$$W_{\vartheta,\gamma}(\hat{\mathbf{e}}) = \begin{cases} W_\vartheta(\hat{\mathbf{e}}), & \hat{\mathbf{e}} \in \mathbf{\Xi}_0 \\ W_\gamma(\hat{\mathbf{e}}), & \hat{\mathbf{e}} \in \mathbf{\Xi}_\infty. \end{cases} \tag{20}$$

Based on Lemma 1 and the constructed homogeneous Lyapunov functions defined in (20), we can obtain the following theorem.

Theorem 1: Consider system (8) under Assumption 1, if the FSGESO is designed as (9), and ω_0 satisfies that $\omega_0 > \max\{(4 d_{\max}^{(n-1)} \sqrt{S_{n,n}})^{1/n}, 1\}$, then there exists $\varepsilon_1 > 0$, for all $\vartheta \in (1 - \varepsilon_1, 1)$ and $\gamma \in (1, 1 + \varepsilon_1)$, the estimation errors $\hat{e}_i (i = 1, 2, \ldots, n)$ are bound and $\hat{e}_1$ can converge to the switching point $|\hat{e}_1| = \delta$ in a fixed-time independent of the initial conditions.

Proof: By making the transformation $\bar{\mathbf{e}} = \Delta_{\omega_0} \hat{\mathbf{e}}$ with $\Delta_{\omega_0} \triangleq \operatorname{diag}(1, 1/\omega_0, \ldots, 1/\omega_0^{n-1})$, the estimation error differential equation (13) can be rewritten as

$$\dot{\bar{\mathbf{e}}} = \omega_0(\mathbf{A}\bar{\mathbf{e}} - \mathbf{\Phi}(1, \mathbf{K}, \vartheta, \gamma, \hat{e}_1)) + \Delta_{\omega_0} \mathbf{D} d^{(n-1)}. \tag{21}$$

The right-hand side of (21) can be divided into two parts, $\omega_0(\mathbf{A}\bar{\mathbf{e}} - \mathbf{\Phi}(1, \mathbf{K}, \vartheta, \gamma, \hat{e}_1))$ and $\Delta_{\omega_0} \mathbf{D} d^{(n-1)}$, respectively. Lemmas 2 and 3 are given first for the derivatives of $W_{\vartheta,\gamma}(\bar{\mathbf{e}})$ with respect to these two vector fields in the Appendix. Then, using the Lemmas 2 and 3, we can get that there exists $\varepsilon_1 > 0$, for all $\bar{\mathbf{e}} \in \mathbb{R}^n$, $\vartheta \in (1 - \varepsilon_1, 1)$, $\gamma \in (1, 1 + \varepsilon_1)$, and $\omega_0 \geqslant 1$, there has

$$\begin{aligned} \dot{W}_{\vartheta,\gamma}(\bar{\mathbf{e}})|_{(21)} \leqslant & -\frac{\omega_0}{2} \varphi\left(\frac{1+\vartheta}{2}, \frac{1+\gamma}{2}, W_{\vartheta,\gamma}(\bar{\mathbf{e}})\right) \\ & + M\sqrt{W_{\vartheta,\gamma}(\bar{\mathbf{e}})} \end{aligned} \tag{22}$$

where $M = 2 d_{\max}^{(n-1)} \sqrt{S_{n,n}} / \omega_0^{n-1}$.

When $d^{(n-1)} = 0$, inequality (22) is expressed as

$$\begin{cases} \dot{W}_{\vartheta,\gamma}(\bar{\mathbf{e}})|_{(21)} \leqslant -\frac{\omega_0}{2}(W_{\vartheta,\gamma}(\bar{\mathbf{e}}))^{\frac{1+\vartheta}{2}}, \bar{\mathbf{e}} \in \mathbf{\Xi}_0 \\ \dot{W}_{\vartheta,\gamma}(\bar{\mathbf{e}})|_{(21)} \leqslant -\frac{\omega_0}{2}(W_{\vartheta,\gamma}(\bar{\mathbf{e}}))^{\frac{1+\gamma}{2}}, \bar{\mathbf{e}} \in \mathbf{\Xi}_\infty. \end{cases} \tag{23}$$

According to (23), we can obtain that, when $\bar{\mathbf{e}}(0) \in \mathbf{\Xi}_\infty$, $W_{\vartheta,\gamma}(\bar{\mathbf{e}})$ converges to $\bar{\mathbf{e}} \in \mathbf{\Xi}_0$ within fixed time $\tau_1 = 4/\omega_0(\gamma - 1)$, and then converges to the origin within fixed time $\tau_2 = 4/\omega_0(1 - \vartheta)$.

When $d^{(n-1)} \neq 0$, according to [23, Lemma 5], there exists ζ and τ_3 independent of the initial conditions, for all $t \geqslant \tau_3$ that

$$W_{\vartheta,\gamma}(\bar{\mathbf{e}}) \leqslant D_1 \exp(-\zeta(t - \tau_3)) + D_2 \tag{24}$$

where $D_1 = 1 - D_2$, $D_2 = (\frac{2M}{\omega_0})^{2/\vartheta}$, $\tau_3 = 4/((\gamma - 1)(\omega_0 - 2M))$, $\zeta = |\max\{-\frac{M\vartheta}{2}(\frac{\omega_0}{2M})^{\vartheta}, \frac{M - \omega_0/2}{1 - (2M/\omega_0)^{2/\vartheta}}\}|$.

Then, according to (24), we can obtain equation (26) shown at the bottom of next page,

$$|\hat{e}_i| = \omega_0^{i-1}|\bar{e}_i| \leqslant \omega_0^{i-1} \|\bar{\mathbf{e}}\| < Y_i, i = 1, 2, \ldots, n \tag{25}$$

where Y_i shows at the bottom of the next page. This indicates that, within a fixed time independent of the initial conditions, the estimation errors can approach a narrow vicinity around the equilibrium point, which theoretically can be made infinitely small by increasing the value of ω_0. Therefore, we can choose $\delta > Y_1$, then the FSGESO can converge to the switching point $|\hat{e}_1| = \delta$ in a fixed time τ_3.

Case 2: When $|\hat{e}_1| < \delta$, the FSGESO will switch to an LGESO. Combining (8) and (9), the differential equation of the

estimation error can be expressed as

$$\dot{\hat{\mathbf{e}}} = (\mathbf{A} - \mathbf{LC})\hat{\mathbf{e}} + \mathbf{D}d^{(n-1)} \tag{27}$$

where

$$\begin{aligned}\mathbf{L} &= \begin{bmatrix}\beta_1 & \beta_2 & \cdots & \beta_n\end{bmatrix}^T \\ &= \begin{bmatrix}\frac{k_1\omega_0}{\delta^{1-\vartheta}_1} & \frac{k_2\omega_0^2}{\delta^{1-\vartheta}2} & \cdots & \frac{k_n\omega_0^n}{\delta^{1-\vartheta}_n}\end{bmatrix}^T \\ &= \begin{bmatrix}k_1\frac{\omega_0}{\delta^{1-\vartheta}} & k_2\left(\frac{\omega_0}{\delta^{1-\vartheta}}\right)^2 & \cdots & k_n\left(\frac{\omega_0}{\delta^{1-\vartheta}}\right)^n\end{bmatrix}^T. \end{aligned} \tag{28}$$

According to (11), the observer gain $\mathbf{K}$ can be chosen as

$$k_i = \frac{n!}{i!(n-i)!}, i = 1, 2, \ldots, n. \tag{29}$$

Obviously, $\mathbf{A} - \mathbf{LC}$ is a Hurwitz matrix whose eigenvalues are all negative real number $-\omega_0/\delta^{1-\vartheta}$. Therefore, we can get that $\hat{\mathbf{e}}$ is asymptotically stable if $d^{(n-1)} = 0$, and $\hat{\mathbf{e}}$ is bounded-input bounded-output (BIBO) stable if $d^{(n-1)} \neq 0$ but it is bounded.

According to the discussion of Cases 1 and 2, the proposed FSGESO is globally convergent. When $|\hat{e}_1| \geq \delta$, the proposed FSGESO is a nonlinear FGESO, which can converge to the switching point in a fixed time independent of the initial conditions. When $|\hat{e}_1| < \delta$, the FSGESO will switch to an LGESO, which can improve the steady-state performance by reducing the sensitivity to system high-frequency disturbance and noise.

Remark 1: For the conventional LGESO, it can only asymptotically converge in an infinite domain. For the conventional FGESO, its bandwidth can be improved by decreasing ϑ, whereas the chattering is more likely to be triggered at the same time. For the proposed FSGESO, due to the chattering is attenuated by using the linear/nonlinear switching strategy, we can set smaller ϑ to obtain higher bandwidth, meanwhile, the steady-state performance of the FSGESO can be ensure by switching the FGESO into LGESO during system steady-state. Therefore, the proposed FSGESO has better dynamic and steady-state performance than the conventional LGESO and FGESO.

B. Design of the SQRC Controller

The CQRC is widely used in practical systems which can be presented as

$$G_{\text{CQRC}}(s) = \frac{2k_r\omega_c s}{s^2 + 2\omega_c s + \omega_h^2} \tag{30}$$

where ω_h is the resonant frequency, ω_c is the cut-off frequency, and k_r is the resonant gain.

However, the CQRC has side effect of the resonant terms during system dynamics [31]. Thus, we proposed an SQRC by using the switching resonant mode to avoid this problem, which

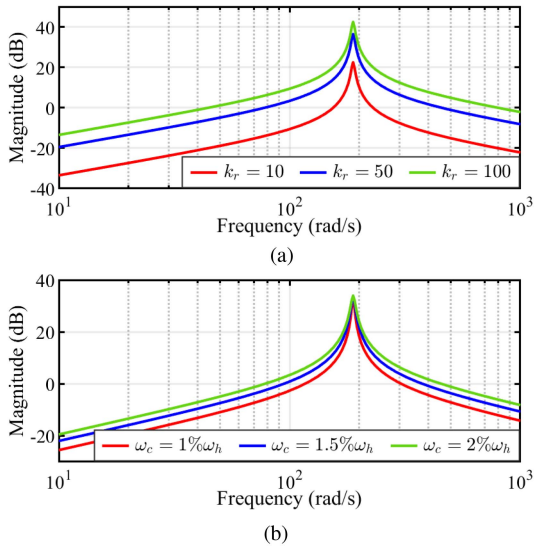

Fig. 1. Bode plots of the SQRC with the varying parameters. (a) $\omega_c = 1.5\%\omega_h, k_r = [10, 50, 100]$. (b) $k_r = 50, \omega_c = [1.0\%\omega_h, 1.5\%\omega_h, 2.0\%\omega_h]$.

can be presented as

$$G_{\text{SQRC}}(s) = \frac{2k_r\omega_c s}{s^2 + 2\omega_c s + \omega_h^2} \cdot \frac{\text{sign}(|e| + \delta) - \text{sign}(|e| - \delta)}{2} \tag{31}$$

where $e = \omega_{m,\text{ref}} - \omega_m$ is the speed error, $\omega_{m,\text{ref}}$ is the speed reference, δ is the switching point, which is used to switch ON or OFF of the SQRC. When the system is in the dynamic process, $|e| \geq \delta$, the SQRC has no effect on the system. When the system approaches steady state, $|e| < \delta$, the SQRC acts on the system to suppress the speed fluctuations caused by the periodic disturbances.

Remark 2: The SQRC is designed by the automatic switching resonant mode to avoid the side effect of resonant controller during motor dynamics. Therefore, the SQRC has the better ability than the CQRC during motor dynamics, while still has the same ability to suppress the periodic disturbance as the CQRC during motor steady-state.

Then, in order to illustrate the effect of the parameters on the performance of the SQRC, Fig. 1 shows the Bode plots of the SQRC with ω_c varies from $1\%\omega_h$ to $2\%\omega_h$ and k_r varies from 10 to 100 when $\omega_h = 60\pi$ rad/s, respectively. Fig. 1(a) illustrates that a larger resonant gain k_r can improve the harmonics suppression capability of the SQRC. However, it is important to note that setting an excessively high resonant gain may amplify the signals near the resonant frequency, potentially leading to instability. In contrast, Fig. 1(b) shows that a larger cut-off frequency ω_c provides a wider gain bandwidth, which can enhance the stability of the system.

$$Y_i = \sqrt{\left(\omega_0^{2(i-1)/r_n(\vartheta)} D_1 \exp(-\zeta(t - T_3) + \omega_0^{2(i-1)/r_n(\vartheta) - 2n/\vartheta}\left(4d_{\max}^{(n-1)}\sqrt{S_{n,n}}\right)^{2/\vartheta}\right)^{r_n(\vartheta)}/\lambda_{\min}(S)} \tag{26}$$

TABLE II
PARAMETERS OF PMSM

Symbol	Quantity	Value
ψ_f	Flux linkage	0.29 Wb
J	Inertia	0.0425 kg·m^2
B	Viscous friction coefficient	0.02 N·m·s
n_p	Pole pairs	3
slot	Slot	12
R_s	Stator resistance	0.675 Ω
L_s	Stator inductance	0.0065 H
P_N	Rated power	5.5 kW
ω_N	Rated speed	3000 r/min
T_N	Rated torque	17.5 N·m
U_N	Rated voltage	380 V
U_{DC}	DC-bus voltage	560 V

C. Design of the Proposed FSGESO-SQRC for PMSM

Although, increasing the order of the GESO can improve the estimation precision towards fast-varying disturbances [33]. However, as reported in [4], this improvement comes at the expense of increased sensitivity to noise. Therefore, the order of the proposed FSGESO is selected as $n = 3$ to balance the disturbance suppression capability and antinoise capability. Then, the FSGESO for the PMSM system is designed as

$$\begin{cases} \dot{\hat{x}}_1 = \hat{x}_2 + b_0 u + k_1\omega_0\psi(\delta, \vartheta_1, \gamma_1, \hat{e}_1) \\ \dot{\hat{x}}_2 = \hat{x}_3 + k_2\omega_0^2\psi(\delta, \vartheta_2, \gamma_2, \hat{e}_1) \\ \dot{\hat{x}}_3 = k_3\omega_0^3\psi(\delta, \vartheta_3, \gamma_3, \hat{e}_1) \end{cases} \tag{32}$$

where $k_1 = 3$, $k_2 = 3$, and $k_3 = 1$.

According to the analysis of the periodic disturbances in Section II, the speed fluctuations in PMSM are mainly caused by first, second, $6n$th, and nN_cth periodic disturbances. Low-frequency speed fluctuations are significant factors that deteriorate the performance of the PMSM drive system in practical applications. Conversely, high-frequency speed fluctuations can typically be disregarded since their effects can be mitigated through the rotor inertia and velocity measurements [31]. Consequently, this article only considers the fundamental frequency of the flux harmonics, inverter nonlinearity, and cogging torque. In addition, based on the number of the pole pairs and slot presented in Table II, it can be observed that the period of cogging torque aligns with that of flux harmonics. As a result, the SQRC only considers first, second, and sixth speed fluctuations, can be designed as

$$\begin{aligned} G'_{\mathrm{SQRC}}(s) = &\left(\frac{2k_{r1}\omega_{c1}s}{s^2 + 2\omega_{c1}s + \omega_{h1}^2} + \frac{2k_{r2}\omega_{c2}s}{s^2 + 2\omega_{c2}s + \omega_{h2}^2} \right. \\ &\left. + \frac{2k_{r6}\omega_{c6}s}{s^2 + 2\omega_{c6}s + \omega_{h6}^2} \right) \\ &\left(\frac{\mathrm{sign}(|e| + \delta) - \mathrm{sign}(|e| - \delta)}{2} \right) \end{aligned} \tag{33}$$

where k_{r1}, k_{r2}, and k_{r6} are the first, second, and sixth resonant gain, ω_{c1}, ω_{c2}, and ω_{c6} are the first, second, and sixth cut-off frequency, $\omega_{h1} = \omega_e$, $\omega_{h2} = 2\omega_e$, and $\omega_{h6} = 6\omega_e$ are the first, second, and sixth resonant frequency, respectively, $\omega_e = n_p\omega_m$ is the electrical angular speed of PMSM.

Using the error feedback control strategy, the speed control law is designed as

$$u = u_0 + u_{qr} - \frac{\hat{x}_2}{b_0} \tag{34}$$

where $u_0 = k_p(\omega_{m,ref} - \omega_m)$ is the speed error feedback control law, k_p is the proportional coefficient, $u_{qr} = L^{-1}(G'_{\mathrm{SQRC}}(s)E(s))$ is the output of the SQRC, L^{-1} represents the inverse Laplace transform, $E(s)$ is the Laplace transform of $e(t)$.

Subsequently, Fig. 2 presents the structural diagram of the FOC-based PMSM with the proposed FSGESO-SQRC. It is evident from Fig. 2 that the current loop adopts PI controllers that produce stator voltages, whereas the proposed FSGESO-SQRC is utilized in the speed loop to produce the q-axis reference current.

IV. PERFORMANCE ANALYSIS OF FSGESO-SQRC

A. Stability Analysis of the Speed Closed-Loop System

The stability of the FSGESO has been analyzed in Section III-A, and it indicates that the FSGESO can converge to switching point in a fixed-time independent of the initial conditions, and the FSGESO is globally BIBO stable under the lumped disturbance. Then, according to the literature [26], the stability of the speed closed-loop of the PMSM system with the proposed FSGESO-SQRC will be analyzed here. First, substituting the speed control law (34) into the PMSM dynamic system (7), we can get that

$$\begin{aligned} \dot{x}_1 &= d + b_0 k_p(\omega_{m,\mathrm{ref}} - \omega_m) + b_0 u_{qr} - \hat{x}_2 \\ &= b_0 \left\{ k_p + L^{-1}\left[G'_{\mathrm{SQRC}}(s)\right] \right\} (\omega_{m,\mathrm{ref}} - x_1) + \hat{e}_2 \\ &= b_0 \left\{ k_p + L^{-1}\left[G'_{\mathrm{SQRC}}(s)\right] \right\} (\omega_{m,\mathrm{ref}} - x_1) + \hat{e}_2. \end{aligned} \tag{35}$$

According to Theorem 1, the disturbance estimation error $\hat{e}_2$ are bounded. Then, taking the Laplace transform of (35), we can obtain the following transfer functions:

$$\frac{X_1(s)}{\Omega_{m,\mathrm{ref}}(s)} = \frac{b_0\left[k_p + G'_{\mathrm{SQRC}}(s)\right]}{s + b_0\left[k_p + G'_{\mathrm{SQRC}}(s)\right]} \tag{36}$$

$$\frac{X_1(s)}{\hat{E}_2(s)} = \frac{1}{s + b_0\left[k_p + G'_{\mathrm{SQRC}}(s)\right]} \tag{37}$$

where $X_1(s)$, $\Omega_{m,\mathrm{ref}}(s)$, and $\hat{E}_2(s)$ are the Laplace transform of $x_1(t)$, $\omega_{m,\mathrm{ref}}(t)$, and $\hat{e}_2(t)$, respectively. Due to k_p, b_0, k_r (k_{r1}, k_{r2} and k_{r6}), and ω_c (ω_{c1}, ω_{c2} and ω_{c6}) are all positive real number. Therefore, the poles of transfer functions (36) and (37) are in the left half-plane of the complex domain. Therefore, the speed closed-loop system is stable.

B. Speed Tracking Performance Analysis

To analyze the speed tracking performance of the proposed method, from the view of practical engineering, the bode diagrams of the proposed method can clearly show its frequency domain characteristics. However, the FSGESO-SQRC constructed in this article is a linear/nonlinear switching system, its transfer function is difficult to obtain. Therefore, according to the

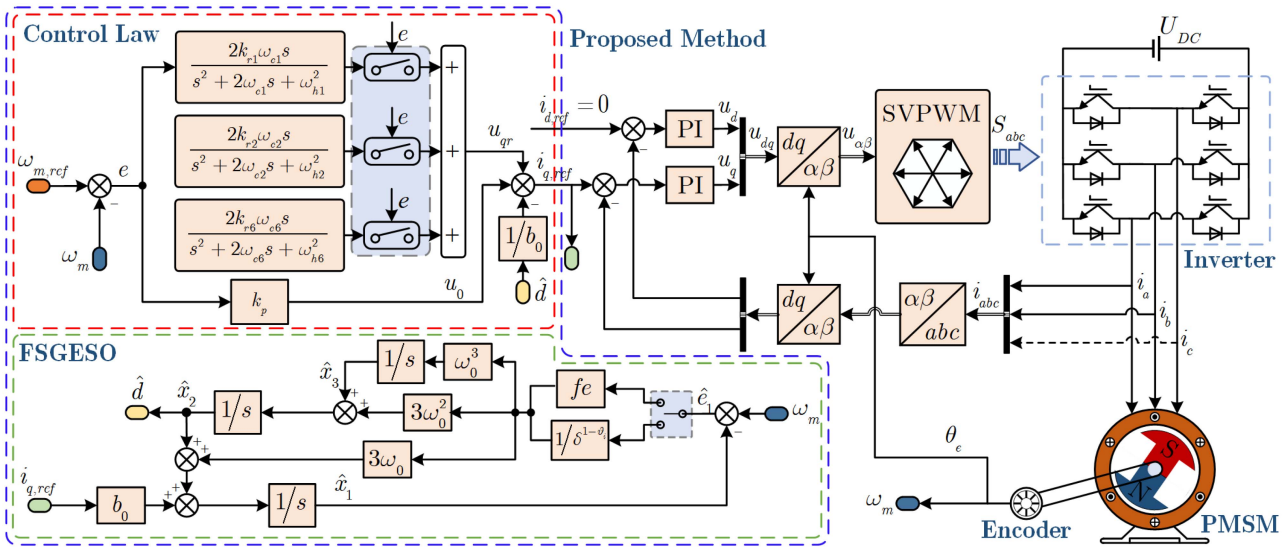

Fig. 2. Structure diagram of the FOC-based PMSM with the proposed FSGESO-SQRC.

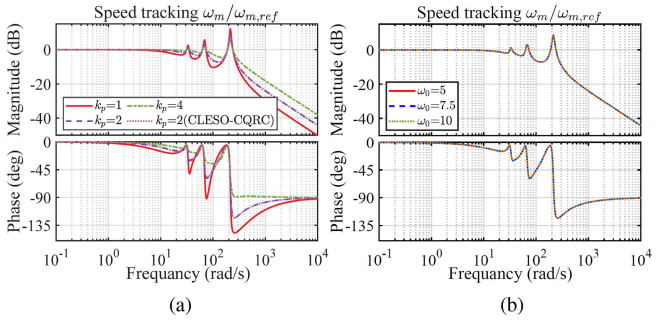

Fig. 3. Bode diagrams of the speed-loop system with different k_p and ω_0. (a) $\omega_0 = 7.5$. (b) $k_p = 2$.

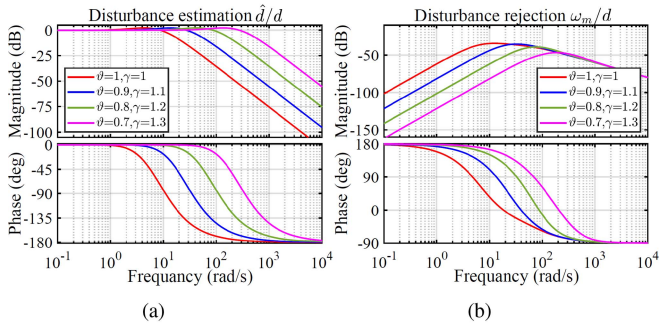

Fig. 4. Bode diagrams of the FSGESO system with different ϑ and γ.

literature [34], a unified frequency-sweep method is adopted to acquire the bode diagrams. Then, selecting $\vartheta = 0.8$, $\gamma = 1.2$, $\omega_{ci} = 1.5\%\omega_{hi}$, and $k_{ri} = 10i$ ($i = 1, 2, 6$), Fig. 3 shows the bode diagrams of the FSGESO-SQRC system with variable k_p and ω_0. It can be seen from Fig. 3 that the bandwidth of the speed loop is only related to the proportional coefficient k_p, and the speed tracking performance improves with the increase of k_p. In addition, Fig. 3(a) shows that the speed tracking performance of the FSGESO-SQRC is the same as CLESO-CQRC with the same k_p.

C. Antidisturbance Performance Analysis

1) Aperiodic Disturbance Suppression: In order to analyze the antidisturbance performance of the proposed method, the bandwidth of the speed loop is designed as 62.8 rad/s, thus, k_p is set as 2.1. In the proposed scheme, the aperiodic disturbance rejection performance is mainly affected by the parameters ϑ, γ, and ω_0. Thus, the bode diagrams of the FSGESO with different ϑ and γ are shown in Fig. 4. It can be seen from Fig. 4, the bandwidth of the FSGESO increases with the decrease of ϑ and increase of γ, and the low-frequency disturbance rejection performance of the FSGESO is stronger under a smaller ϑ and a larger γ. Note that the FSGESO is equivalent to the LGESO when $\vartheta = 1$ and $\gamma = 1$. Meanwhile, to show that the antidisturbance ability of the FSGESO is superior to the CLESO and LGESO, choosing $k_p = 2.1$, $\vartheta = 0.8$, and $\gamma = 1.2$, the comparison of the antidisturbance performance with the three methods is shown in Fig. 5. It can be seen from Fig. 5, the FSGESO has the best disturbance estimation and rejection ability to the low-frequency disturbance with the same parameter ω_0, followed by LGESO and CLESO. In addition, even if the value of parameter ω_0 in the FSGESO is much smaller than CLESO, its low-frequency antidisturbance ability is stronger.

2) Periodic Disturbance Suppression: From Fig. 3(a), we can see that increasing k_p can enhance the antidisturbance capability to the periodic disturbance. However, the restricted current loop bandwidth limits the speed loop bandwidth meaning that k_p cannot be excessively large [29]. Thus, according to Fig. 1, we can set appropriate k_r and ω_c to suppress the special periodic disturbance effectively. Selecting $k_p = 2.1$, $\vartheta = 0.8$, $\gamma = 1.2$, $\omega_0 = 7.5$, $\omega_{ci} = 1.5\%\omega_{hi}$, and $k_{ri} = 10i$ ($i = 1, 2, 6$),

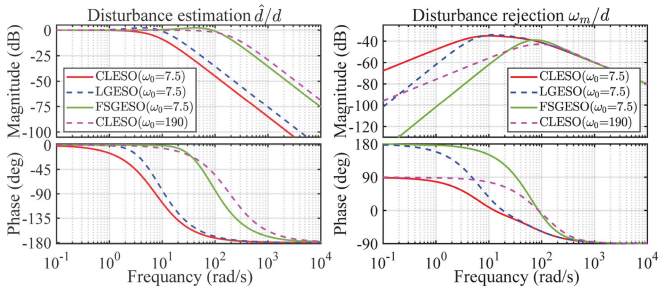

Fig. 5. Comparison of the antidisturbance performance of the CLESO, LGESO, and FSGESO methods.

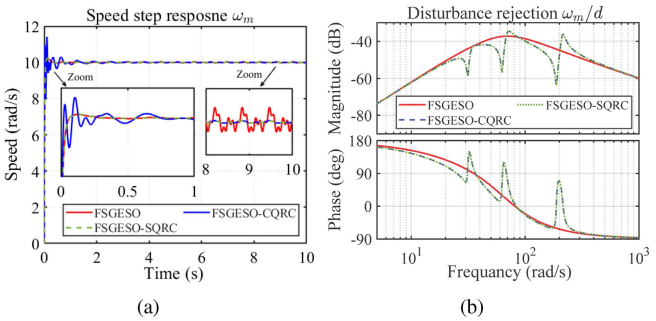

Fig. 6. Step response curves and bode diagrams of the FSGESO, FSGESO-CQRC, and FSGESO-SQRC.

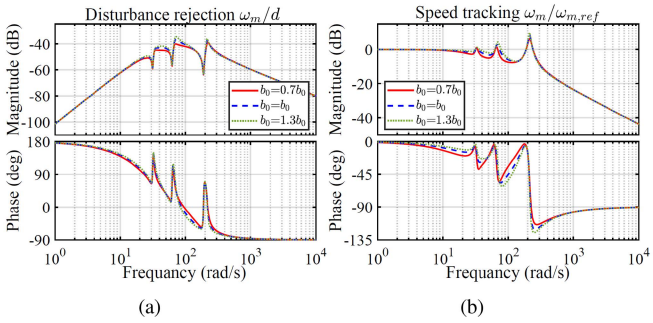

Fig. 7. Bode diagrams of the antidisturbance and speed tracking performance of the FSGESO-SQRC with b_0 varies from $0.7b_0$ to $1.3b_0$.

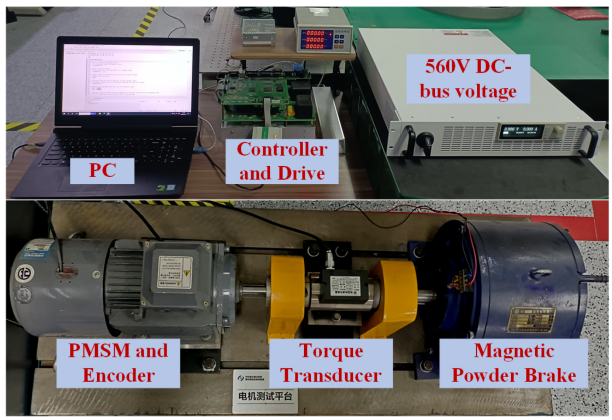

Fig. 8. 5.5 kW PMSM hardware platform.

the step response curves and bode diagrams of the FSGESO, FSGESO-CQRC, and FSGESO-SQRC are shown in Fig. 6. Fig. 6(a) shows that the SQRC avoids the side effect of the resonant controller by using the automatic switching strategy, and the SQRC has better ability than the CQRC during the motor dynamics. Moreover, Fig. 6(b) shows that the SQRC can improve the special periodic disturbance suppression capability, and still has the same ability to suppress the periodic disturbance as the CQRC during motor steady-state.

D. Parameters Robustness Analysis

The inertia J and torque coefficient K_t are affected by operating environment changes and aging to produce mismatches from nominal parameters. However, the proposed method includes model information $b_0 = K_{t0}/J_0$. Thus, it is necessary to analyze the robustness of the FSGESO-SQRC to parameters mismatch. Selecting $k_p = 2.1$, $\vartheta = 0.8$, $\gamma = 1.2$, $\omega_0 = 7.5$, $\omega_{ci} = 1.5\%\omega_{hi}$, and $k_{ri} = 10i$ (i = 1, 2, 6), Fig. 7 shows the bode diagrams of the antidisturbance and speed tracking performance of the FSGESO-SQRC with b_0 varies from $0.7b_0$ to $1.3b_0$. From Fig. 7, it can be seen that the change of parameter b_0 only has a limited impact on the system's antidisturbance and speed tracking performance. Meanwhile, according to (36) and (37), we can obtain that parameter b_0 change will not change the stability of the speed-loop system. Therefore, the proposed FSGESO-SQRC scheme exhibits excellent robustness to parameters variations.

E. Parameters Configuration

The proposed method has some parameters that need to be designed, including k_p, ϑ, γ, ω_0, k_r, ω_c and δ. First, according to the speed tracking performance analysis, the bandwidth of the speed loop is only related to the proportional coefficient k_p, therefore, we can design k_p based on the expected speed loop bandwidth. In this article, we design the bandwidth of the speed loop as 62.8 rad/s, thus, k_p is set as 2.1. Second, according to the analysis in Section IV-C, the antidisturbance performance of the proposed method mainly effected by the parameters ϑ, γ, and ω_0. For ϑ and γ, we can get that a smaller ϑ and a larger γ can achieve better antidisturbance performance to the aperiodic disturbance. However, an overshoot tends to be generated with a large γ, and the chattering is more likely to be triggered with a small ϑ [23]. Although, the proposed FSGESO-SQRC method has deal with the chattering problem of the conventional FGESO by using the linear/nonlinear switching strategy, the ϑ and γ also should not be designed as too small or large. Thus, we set $\vartheta = 0.8$ and $\gamma = 1.2$ for the FSGESO. According to [29], the bandwidth of the FSGESO is recommended to design to be twice the speed loop. Therefore, ω_0 is selected as 7.5. Then, for k_r and ω_c, according to [31], k_r should increase with the increase of the resonant frequency. Thus, k_{r2} and k_{r6} are set to $2k_{r1}$ and $6k_{r1}$, respectively. According to [29], ω_c is set to $1.5\%\omega_h$. Finally, δ is the switching point for the FSGESO-SQRC, it is designed to

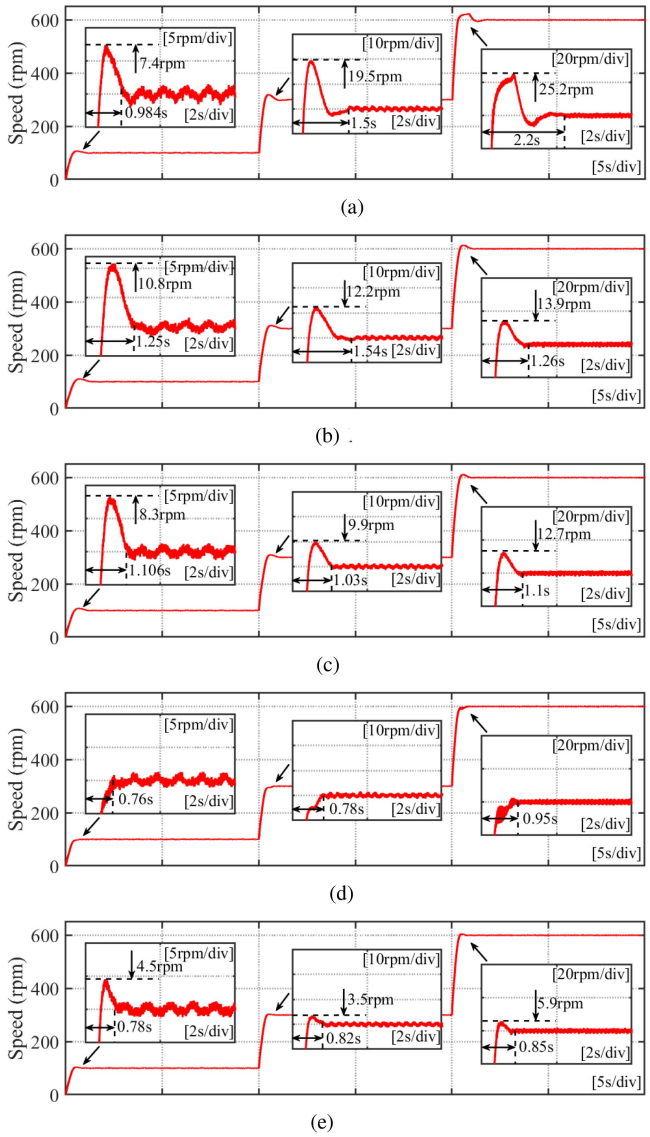

Fig. 9. Experimental results of the speed step responses with the five different algorithms under rated load. (a) PI. (b) LGESO. (c) FGESO. (d) EKF. (e) FSGESO.

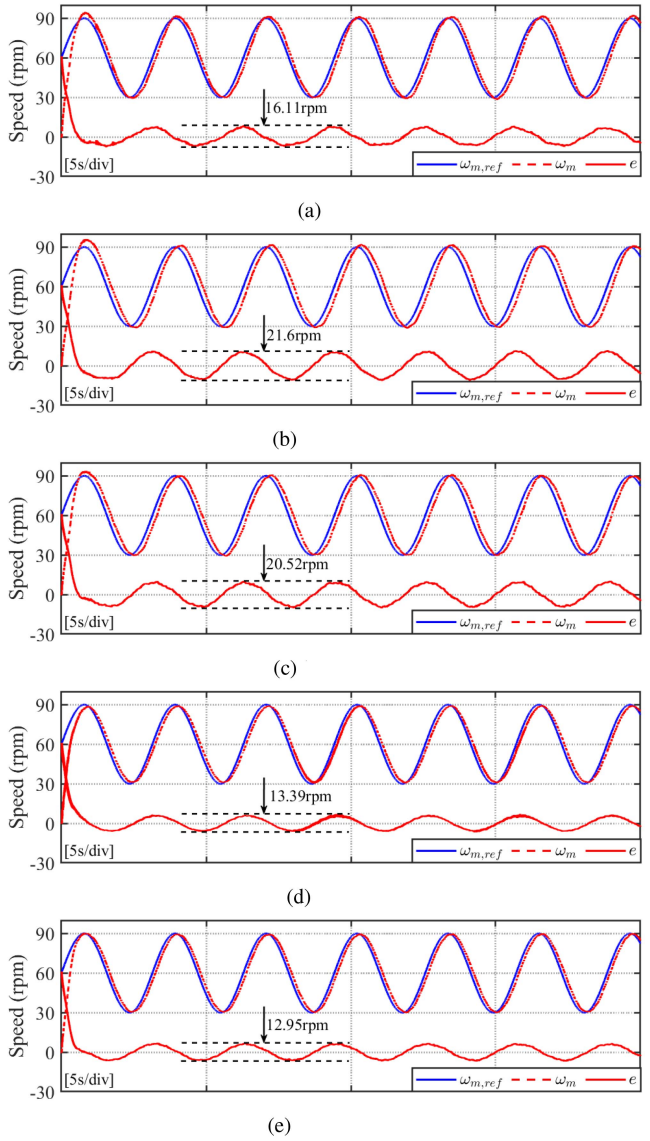

Fig. 10. Experimental results of the speed sinusoidal responses with the five different algorithms under rated load. (a) PI. (b) LGESO. (c) FGESO. (d) EKF. (e) FSGESO.

ensure that the FSGESO switches from FGESO to LGESO to avoid chattering and SQRC avoids the side effect of the resonant controller during motor dynamics. Thus, the value of δ should be selected by the steady-state speed error, which is recommended to select as twice steady-state speed error.

V. Experimental Results and Analysis

To exhibit the effectiveness of the proposed FSGESO-SQRC method, experiments are carried out on a hardware platform with a 5.5 kW PMSM, illustrated in Fig. 8. The crucial nominal parameters of the PMSM are itemized in Table II. During the experiments, the control algorithm is executed on a DSP-TMS320F28335, and a magnetic powder brake is used to add the external load. The current loop of the PMSM adopts PI controller, and the sampling frequency of the current loop is 8 kHz. The parameters of the d- and q-axis current PI controllers are both designed as $k_p = 7.141$ and $k_i = 741.6$. The proposed FSGESO-SQRC strategy is applied as the speed controller whose sampling frequency is the same as the current loop, and the bandwidth of speed loop is designed as 62.8 rad/s. Thus, the parameters of the proposed methods are designed as $k_p = 2.1$, $\vartheta = 0.8$, $\gamma = 1.2$, $\omega_0 = 7.5$, $k_{r1} = 10$, $k_{r2} = 2k_{r1}$, $k_{r6} = 6k_{r1}$, $\omega_{ci} = 1.5\%\omega_{hi}$, $\omega_{hi} = i\omega_e$ (i = 1,2,6), and $\delta = 0.1$. Moreover, conventional PI, LGESO and FGESO methods are also studied under different working conditions on the PMSM hardware platform to compare with the proposed method. Meanwhile, the state-of-the-art EKF is constructed as a benchmark to evaluate whether the proposed method can achieve the performance level of state-of-the-art methods. The bandwidth of the PI speed controller is designed as the same as the proposed FSGESO-SQRC,

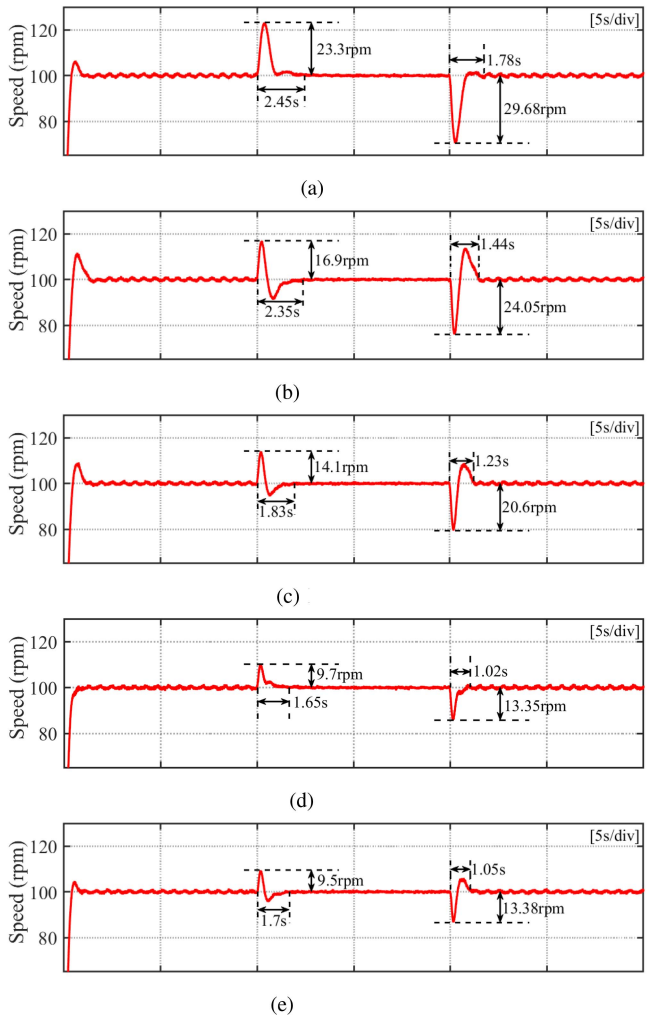

Fig. 11. Experimental results of the five different algorithms with sudden unload and sudden load under rated load. (a) PI. (b) LGESO. (c) FGESO. (d) EKF. (e) FSGESO.

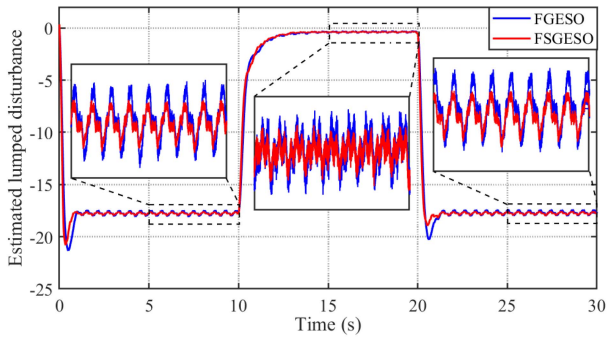

Fig. 12. Estimated lumped disturbance of the FGESO and FSGESO.

thus, $k_{sp} = 1.9$, $k_{si} = 3.4$. The parameters of the LGESO are selected as the same as the proposed FSGESO. According to the literature [23], the parameters ϑ and γ of the conventional FGESO are set as $\vartheta = 0.9, \gamma = 1.1$, and the other parameters are set as the same as the proposed FSGESO. For the EKF, according

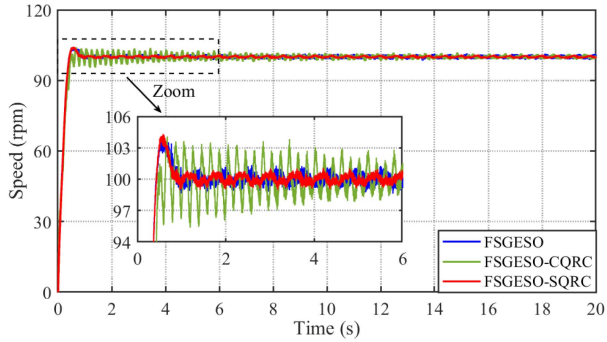

Fig. 13. Speed responses of the FSGESO, FSGESO-CQRC, and FSGESO-SQRC methods to step signal $\omega_{m,\text{ref}} = 100$ r/min under rated load.

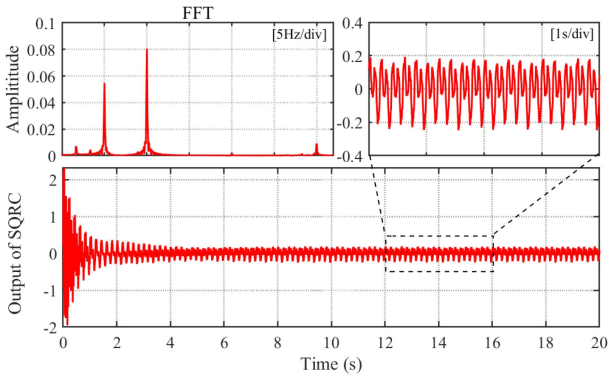

Fig. 14. Output of the SQRC and its FFT analysis results.

to the literature [11], its antidisturbance ability is determined by the gain coefficient of the integral of tracking error, but the EKF gain coefficient is limited by the measurement noise. Therefore, the gain coefficient of the EKF is set to 420, enabling the system to achieve its best dynamics possible.

A. *Dynamic Performance Experiment*

To evaluate the dynamic performance of the proposed method, the comparative experimental results of the PI, LGESO, FGESO, EKF, and FSGESO under rated load are given in Figs. 9 and 10. First, Fig. 9 shows the speed step responses of the five different schemes from 100 to 600 r/min. It can be seen from Fig. 9 that the overshoot and settling time of the FSGESO in the full speed range are smaller than those of the PI, LGESO, and FGESO methods. Therefore, the proposed FSGESO has better dynamic performance than the other three methods under the step responses. Comparing the proposed FSGESO with the state-of-the-art EKF method, the setting time of the FSGESO is similar to that of the EKF, which shows that the proposed method can achieve the performance indicators of the state-of-the-art algorithm. Furthermore, Fig. 10 shows the speed response curves and speed tracking error curves of the five different algorithms with a sinusoidal signal $\omega_{m,\text{ref}} = 60 + 30\sin(2t)$ r/min, respectively. From Fig. 10, it can be seen that the proposed FSGESO outperform PI, LGESO, and FGESO in tracking sinusoidal speed reference. The speed tracking error fluctuations with the

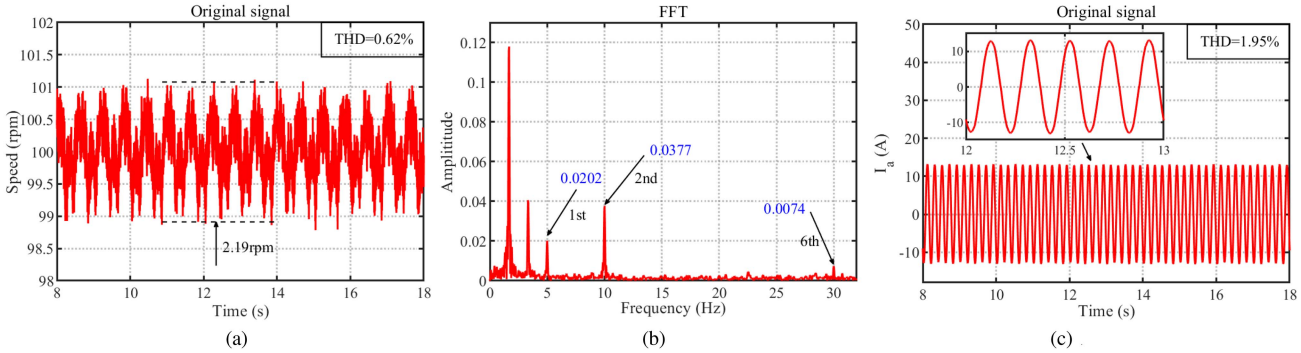

Fig. 15. Experimental results of the FSGESO method with step signal $\omega_{m,\text{ref}} = 100$ r/min under rated load. (a) Speed. (b) Harmonic. (c) A-phase current.

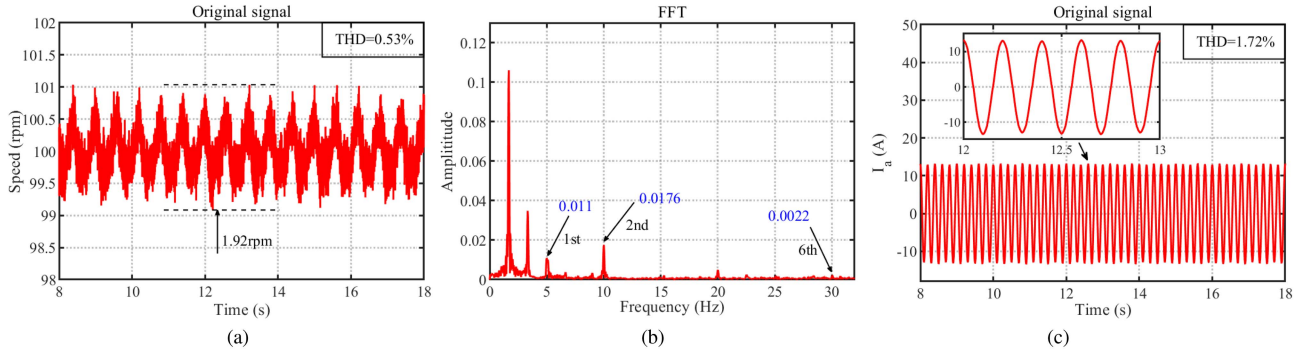

Fig. 16. Experimental results of the FSGESO-SQRC method with step signal $\omega_{m,\text{ref}} = 100$ r/min under rated load. (a) Speed. (b) Harmonic. (c) A-phase current.

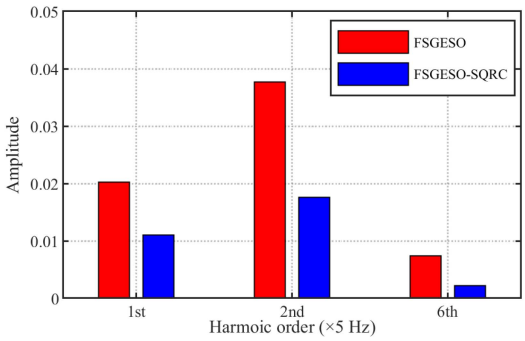

Fig. 17. Histogram of the speed harmonics with $\omega_{m,\text{ref}} = 100$ r/min.

TABLE III
PERFORMANCE COMPARISON OF THE PI, LGESO, FGESO, EKF, AND FSGESO WITH SUDDEN UNLOAD AND SUDDEN LOAD

Control method	Remove rated load		Add rated load	
	Speed rise (r/min)	Setting time (s)	Speed drop (r/min)	Setting time (s)
PI	23.3	2.45	29.68	1.78
LGESO	16.9	2.35	24.05	1.44
FGESO	14.1	1.83	20.6	1.23
EKF	9.7	1.65	13.35	1.02
FSGESO	9.5	1.7	13.38	1.05

five methods are 16.11 r/min, 21.6 r/min, 20.52 r/min, 13.39 r/min, and 12.95 r/min, respectively.

B. Aperiodic Disturbance Suppression Experiment

To verify the antidisturbance performance of the proposed method to aperiodic disturbance, the comparative experiments of the PI, LGESO, FGESO, EKF, and FSGESO are carried out under the condition of sudden unload and sudden load. Then, Fig. 11 shows the experimental results of the five different methods under rated load. When the load is removed abruptly at 10 s, we can obtain from Fig. 11 that the speed rise with the PI, LGESO, FGESO, EKF, and FSGESO algorithms is 23.3 r/min, 16.9 r/min, 14.1 r/min, 9.7 r/min, and 9.5 r/min, respectively, and the settling time of the five different algorithms is 2.45 s, 2.35 s, 1.83 s, 1.65 s, and 1.7 s, respectively. When the load is added suddenly at 20 s, the speed drop with the PI, LGESO, FGESO, EKF, and FSGESO algorithms is 29.68 r/min, 24.05 r/min, 20.6 r/min, 13.35 r/min, and 13.38 r/min, respectively, and the settling time is 1.78 s, 1.44 s, 1.23 s, 1.02 s, and 1.05 s, respectively. Moreover, we have listed the important performance indices of the PI, LGESO, FGESO, EKF, and FSGESO in Table III. Thus, it can be concluded from Fig. 11 and Table III that the proposed method has a stronger antidisturbance performance to aperiodic disturbance than the PI, LGESO, and

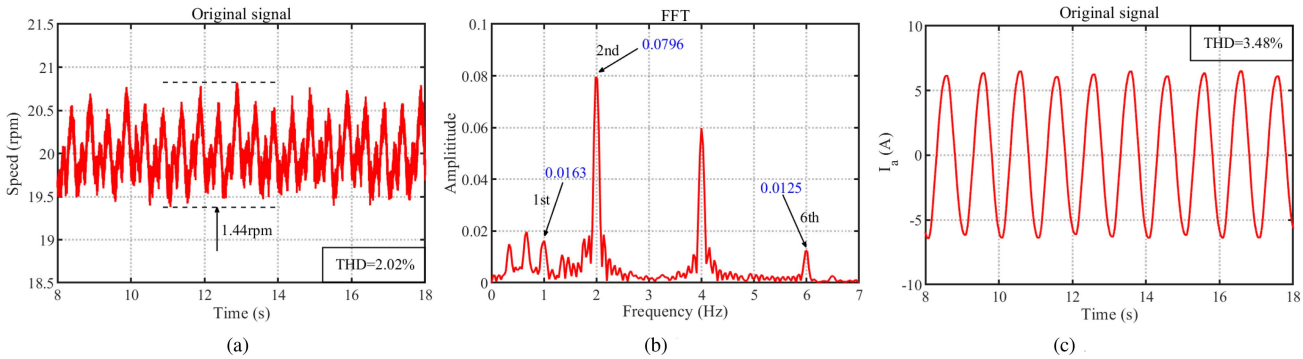

Fig. 18. Experimental results of the FSGESO method with step signal $\omega_{m,\text{ref}} = 20$ r/min under 50% rated load. (a) Speed. (b) Harmonic. (c) A-phase current.

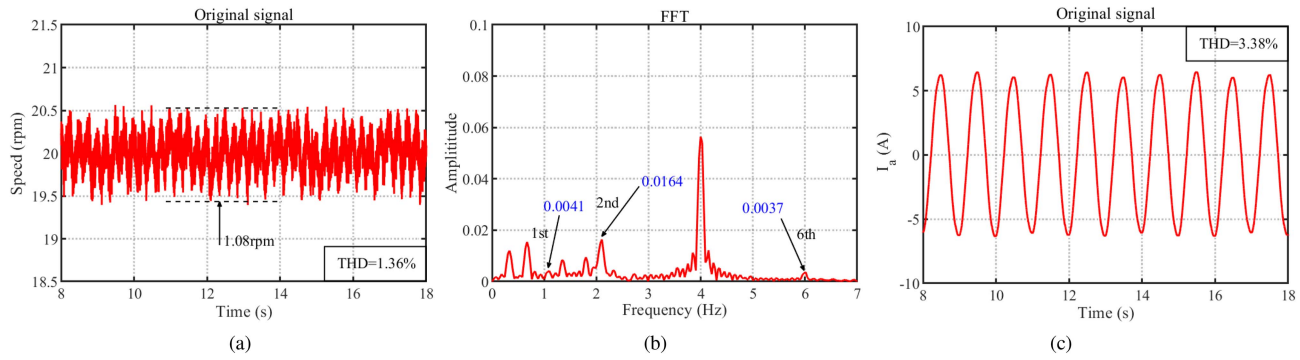

Fig. 19. Experimental results of the FSGESO-SQRC method with step signal $\omega_{m,\text{ref}} = 20$ r/min under 50% rated load. (a) Speed. (b) Harmonic. (c) A-phase current.

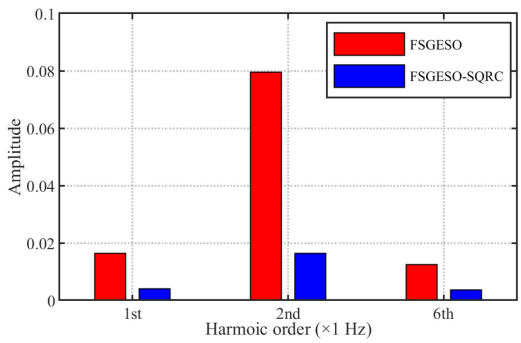

Fig. 20. Histogram of the speed harmonics with $\omega_{m,\text{ref}} = 20$ r/min.

FGESO methods, and the antidisturbance performance of the proposed method reaches the level of state-of-the-art algorithms.

Meanwhile, to illustrate the advantage of the proposed FSGESO compared with the conventional FGESO, Fig. 12 shows the disturbance estimation results of the FGESO and FSGESO under the condition that the load varies from rated load to 0 N·m to rated load. From Fig. 12, we can seen that the FSGESO has a faster response than the FGESO as the load changes. Furthermore, we can clearly see that the steady-state fluctuation of the estimated lumped disturbance with the FSGESO is much smaller than that with the FGESO in the whole process. Therefore, compared with the conventional FGESO, the proposed FSGESO with the linear/nonlinear switching strategy has better dynamic performance and steady-state performance. The dynamic performance of the FSGESO can be improved by adjusting the parameter ϑ, and the steady-state performance can be guaranteed by the switching strategy.

C. Periodic Disturbance Suppression Experiment

In order to evaluate the effectiveness of the proposed FSGESO-SQRC method to suppress the periodic disturbance, comparative experiments are carried out by using the FSGESO and FSGESO-SQRC methods.

First, to show that the proposed SQRC can avoid the side effect of the resonant terms during motor dynamics, the speed responses of the FSGESO, FSGESO-CQRC, and FSGESO-SQRC methods to step signal $\omega_{m,\text{ref}} = 100$ r/min under rated load are shown in Fig. 13. As shown in Fig. 13, comparing the speed response curves of the FSGESO and FSGESO-CQRC, the dynamic process of the FSGESO-CQRC is seriously affected by the addition of CQRC, meanwhile, it still needs a long settling time to eliminate the speed fluctuation caused by the CQRC. In contrast, the speed response curve of the FSGESO-SQRC method is almost the same as the FSGESO, and there is only a small speed fluctuation, which can be quickly eliminated when it will reach the steady state. Therefore, compared with the CQRC,

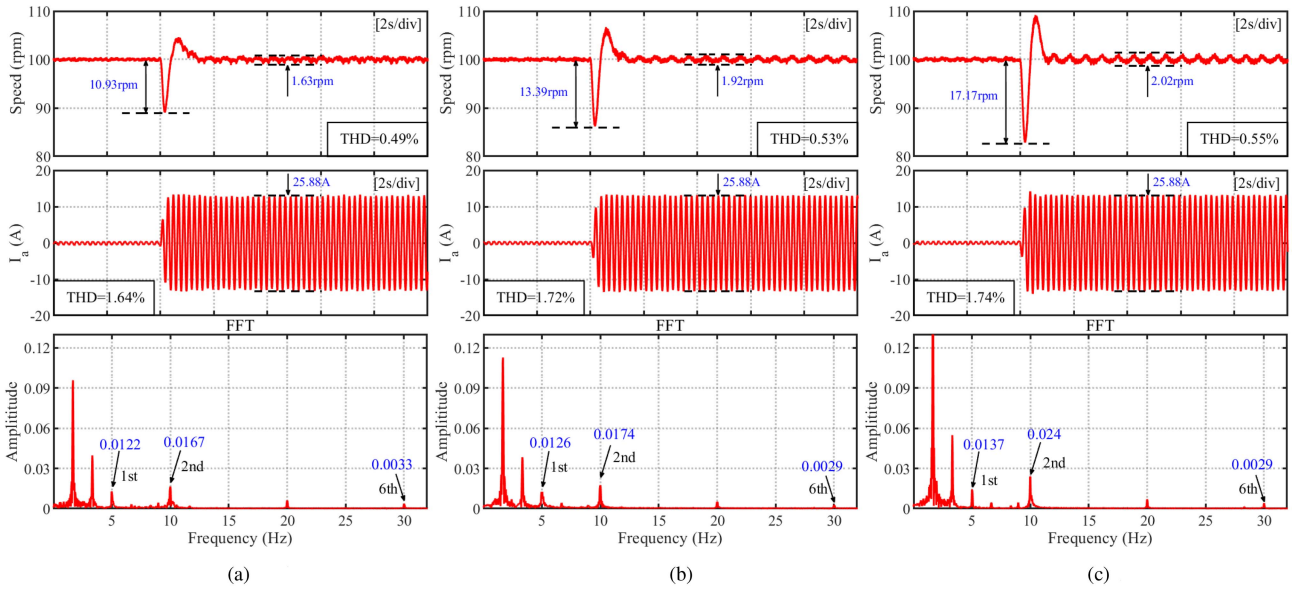

Fig. 21. Experimental results of the FSGESO-SQRC method with b_0 variation. (a) $0.7b_0$. (b) b_0. (c) $1.3b_0$.

the SQRC proposed in this article has little side effect of the resonant terms during motor dynamics, which can be eliminated quickly. In addition, Fig. 14 shows the output of the SQRC and its fast Fourier transform (FFT) analysis results corresponding to the experimental result of the FSGESO-SQRC method of Fig. 13. It can be seen from Fig. 14 that the first, second, and sixth harmonics have been effectively extracted by the SQRC.

Then, in order to assess the effectiveness of the FSGESO-SQRC in mitigating periodic disturbances, the speed fluctuations caused by the periodic disturbances are analyzed using the fast Fourier transform (FFT). The speed responses of the FSGESO and FSGESO-SQRC methods to step signal $\omega_{m,\text{ref}} = 100$ r/min under rated load have shown in Fig. 13. Subsequently, we use the steady-state speed data collected between 8 and 18 s for FFT analysis, which enables us to identify the first, second, and sixth harmonics. Figs. 15 and 16 have shown the steady-state speed response, FFT analysis of speed, and A-phase current of the FSGESO and FSGESO-SQRC methods, respectively. As shown in Figs. 15(a) and 16(a), the fluctuation and total harmonic distortion (THD) of the steady-state speed with the FSGESO are 2.19 r/min and 0.62%, the fluctuation and THD of the steady-state speed with the FSGESO-SQRC are reduced to 1.92 r/min and 0.53% by adding the SQRC to speed loop. Moreover, Fig. 15(b) shows that the first, second, and sixth speed harmonics with the FSGESO are 0.0202 r/min, 0.0377 r/min, and 0.0074 r/min, respectively. When the SQRC is applied to the FSGESO, the first, second, and sixth speed harmonics with the FSGESO-SQRC decrease to 0.011 r/min, 0.0176 r/min, and 0.0022 r/min, respectively. Meanwhile, Fig. 17 exhibits a histogram depicting the discrepancies in harmonic amplitude outcomes. Clearly, the FSGESO-SQRC has a satisfactory capability for periodic disturbance suppression. Finally, Figs. 15(c) and 16(c) show that the THD of the I_a with the FSGESO and the FSGESO-SQRC is 1.95% and 1.72%, respectively, which is further verified that the proposed method makes the speed smoother. In summary, it can be concluded that the FSGESO-SQRC method effectively attenuates the first, second, and sixth speed harmonics caused by the periodic disturbances by using the SQRC, thereby reducing the THD of the steady-state speed and speed fluctuation.

Considering that the torque fluctuation of PMSM is more obvious at low speed, we conduct experiments at a low speed of $\omega_{m,\text{ref}} = 20$ r/min under 50% rated load. Figs. 18 and 19 have shown the steady-state speed response, FFT analysis of speed and A-phase current of the FSGESO and FSGESO-SQRC methods, respectively. Upon compensating for the FSGESO method using the SQRC, the THD of the speed reduces from 2.02% to 1.36%. Figs. 18(b) and 19(b) show that the first, second, and sixth harmonics decrease from 0.0163 r/min, 0.0796 r/min, and 0.0125 r/min to 0.0041 r/min, 0.0164 r/min, and 0.0037 r/min, respectively. And Fig. 20 exhibits a histogram depicting the discrepancies in harmonic amplitude outcomes. In addition, the A-phase current exhibits smoother performance after the implementation of the SQRC.

D. Parameters Robustness Experiment

In order to verify the parameters robustness of the proposed FSGESO-SQRC method, Fig. 21 shows the experimental results of the FSGESO-SQRC method with the parameter b_0 variation. In Fig. 21, speed, A-phase current and Fourier analysis of steady-state speed are presented from top to bottom, respectively. According to (32) and (34), the parameter robustness of the proposed method is only related to parameter $b_0 = K_{t0}/J_0$, which is the function of the torque coefficient K_{t0} and inertia J_0. Therefore, we can selected b_0 as the tested parameter to verify the robustness of the proposed method in the case of torque coefficient K_{t0} and inertia J_0 mismatches, and we set b_0 from $0.7b_0$ to $1.3b_0$. Then, it can be seen from Fig. 21, the proposed method still has strong antidisturbance performance to

TABLE IV
COMPARISON OF THE EXECUTION TIME

Methods	Clock cycles	Execution time
PI	773	5.15 μs
LGESO	845	5.63 μs
FGESO	1175	7.83 μs
EKF	1251	8.34 μs
FSGESO-SQRC	1482	9.88 μs

aperiodic and periodic disturbances with the parameter variation. Therefore, we can conclude that the proposed FSGESO-SQRC has strong robustness to parameter variation.

E. Computational Burden Analysis

In order to discuss the computational burden of the proposed method, the comparison of the execution time of the five methods on DSP is given in Table IV. The clock frequency of the 32-bit floating-point DSP-TMS320F28335 is 150 MHz. Therefore, the execution time can be calculated based on the clock cycles performed by the algorithm. It can be seen from Table IV that the execution time of the PI, LGESO, FGESO, EKF, and FSGESO-SQRC is 5.15 μs, 5.63 μs, 7.83 μs, 8.34 μs, and 9.88 μs, respectively. The shortest execution time is for PI, followed by LGESO, FGESO, and EKF, while the longest is for the proposed method. Fortunately, the execution time of the proposed scheme is much shorter than the 125 μs control period of the speed loop, which is acceptable for PMSM speed control.

VI. CONCLUSION

In this article, a fixed-time switching generalized ADRC with an SQRC is proposed to enhance the speed control performance of PMSM. First, an FSGESO is designed to estimate the aperiodic disturbance in a fixed time and compensate the disturbance to the feedback control law. Comparing with the conventional LGESO and FGESO, the FSGESO has better dynamic and steady-state performance by combining the advantages of the FGESO and LGESO. Second, an SQRC is designed to suppress the periodic disturbance in parallel with the FSGESO, which has a wider gain bandwidth by tuning the cut-off frequency. Meanwhile, the SQRC has little side effect of the resonant terms during the motor dynamics by using the automatic switching resonant mode. Then, the performance analysis of the proposed FSGESO-SQRC has been given systematically. Finally, the experimental results show that the FSGESO-SQRC method is feasible and effective for PMSM system and has satisfactory dynamic and steady-state speed control performance under the aperiodic and periodic disturbances, reaching the performance level of state-of-the-art methods.

APPENDIX

Notation 1: $\mathbb{R}_+ = \{x \in \mathbb{R} | x \geqslant 0\}$ and $\mathbb{R}_+^* = \{x \in \mathbb{R} | x > 0\}$; $\mathbf{\Lambda}_\lambda^{\mathbf{r}} \triangleq \text{diag}(\lambda^{r_1}, \lambda^{r_2}, \cdots, \lambda^{r_n})$ for all $\lambda \in \mathbb{R}_+$, and $\mathbf{r} = [r_1 \quad r_2 \quad \cdots \quad r_n]^T$ with $r_i \in \mathbb{R}_+ (i = 1, 2, \cdots, n)$; $\lambda_{\min}(\mathbf{S})$ is the smallest eigenvalue of $\mathbf{S}$, $S_{i,j}$ is the element of the ith row and the jth column of $\mathbf{S}$.

Definition 1 (see [18]): Let $\mathbf{f} : \mathbb{R}_+ \times \mathbb{R}^n \to \mathbb{R}^n$ be a continuous vector field satisfies $\mathbf{f}(\mathbf{0}) = \mathbf{0}$. Consider the system as follows:

$$\dot{\mathbf{x}}(t) = \mathbf{f}(\mathbf{x}(t)), \mathbf{x}(\mathbf{0}) = \mathbf{x}_0. \tag{38}$$

System (38) is said to be fixed-time stable if it is globally finite-time stable and the settling-time function $T(\mathbf{x}_0)$, i.e., $\exists T_{\max} > 0$ such that $T(\mathbf{x}_0) < T_{\max}$ for all $\mathbf{x}_0 \in \mathbb{R}^n$.

Definition 2 (see [22]): A function $f(\mathbf{x}) : \mathbb{R}^n \to \mathbb{R}$ is homogeneous of degree d with respect to the weight $\mathbf{r}$ if $f(\mathbf{\Lambda}_\lambda^{\mathbf{r}} \mathbf{x}) = \lambda^d f(\mathbf{x})$ for all $\mathbf{x} \in \mathbb{R}^n$ and $\lambda > 0$. A vector field $\mathbf{f} : \mathbb{R}^n \to \mathbb{R}^n$ is homogeneous of degree d with respect to the weight $\mathbf{r}$ if the ith component f_i is homogeneous of degree $r_i + d$ with respect to the weight $\mathbf{r}$ for all $0 \leqslant i \leqslant n$. A dynamical system $\dot{\mathbf{x}} = \mathbf{f}(\mathbf{x})$ is homogeneous of degree d with respect to the weight $\mathbf{r}$ if the vector field $\mathbf{f}$ is homogeneous of degree d with respect to the weight $\mathbf{r}$.

Definition 3 (see [17]): A function $f(\mathbf{x}) : \mathbb{R}^n \to \mathbb{R}$ is said homogeneous in the p-limit ($p = 0$ or ∞) with associated triple $(\mathbf{r}_p, d_p, f_p)$, where $\mathbf{r}_p \in (\mathbb{R}_+^*)^n$ is the weight, $d_p \in \mathbb{R}_+$ is the degree and $f_p(\mathbf{x}) : \mathbb{R}^n \to \mathbb{R}$ is the approximating function, if $f(\mathbf{x})$ is continuous, $f_p(\mathbf{x})$ is continuous and not identically zero, and for each compact set $\mathbf{C} \in \mathbb{R}^n \backslash \{0\}$ and each $\varepsilon_p > 0$, there exists λ_p such that

$$\begin{cases} \max\limits_{\mathbf{x} \in \mathbf{C}} \left| f(\mathbf{\Lambda}_\lambda^{\mathbf{r}_0} \mathbf{x}) / \lambda^{d_0} - f_0(\mathbf{x}) \right| \leqslant \varepsilon_0, \lambda \in (0, \lambda_0] \\ \max\limits_{\mathbf{x} \in \mathbf{C}} \left| f(\mathbf{\Lambda}_\lambda^{\mathbf{r}_\infty} \mathbf{x}) / \lambda^{d_\infty} - f_\infty(\mathbf{x}) \right| \leqslant \varepsilon_\infty, \lambda \in [\lambda_\infty, \infty). \end{cases} \tag{39}$$

A vector field $\mathbf{f} : \mathbb{R}^n \to \mathbb{R}^n$ is said homogeneous in the p-limit ($p = 0$ or ∞) with associated triple $(\mathbf{r}_p, d_p, \mathbf{f}_p)$, where $\mathbf{r}_p \in (\mathbb{R}_+^*)^n$ is the weight, $d_p \in \mathbb{R}$ is the degree, and $\mathbf{f}_p$ is the approximating vector field, if f_i is homogeneous in the p-limit ($p = 0$ or ∞) with associated triple $(\mathbf{r}_p, d_p + r_{p,i}, f_{p,i})$ for all $0 \leqslant i \leqslant n$ and $d_p + r_{p,i} \geqslant 0$.

A function $f(\mathbf{x}) : \mathbb{R}^n \to \mathbb{R}$ (or a vector field $\mathbf{f} : \mathbb{R}^n \to \mathbb{R}^n$) is said homogeneous in the bi-limit if it is homogeneous in the 0-limit and ∞-limit.

Lemma 2: There exists $\varepsilon_1 \in (0, \varepsilon)$, ε is defined in Lemma 1, for all $\bar{\mathbf{e}} \in \mathbb{R}^n$, $\vartheta \in (1 - \varepsilon_1, 1)$ and $\gamma \in (1, 1 + \varepsilon_1)$, there has

$$\begin{aligned} &\langle dW_{\vartheta,\gamma}(\bar{\mathbf{e}}) / d\bar{\mathbf{e}}, A\bar{\mathbf{e}} - \mathbf{\Phi}(1, \mathbf{K}, \vartheta, \gamma, \hat{e}_1) \rangle \\ &\leq -\frac{1}{2} \varphi \left(\frac{1 + \vartheta}{2}, \frac{1 + \gamma}{2}, W_{\vartheta,\gamma}(\bar{\mathbf{e}}) \right). \end{aligned} \tag{40}$$

Proof: Inequality (40) is equivalent to

$$\begin{cases} \langle dW_\vartheta(\bar{\mathbf{e}}) / d\bar{\mathbf{e}}, A\bar{\mathbf{e}} - \mathbf{\Phi}(1, \mathbf{K}, \vartheta, \gamma, \hat{e}_1) \rangle \\ \qquad \leq -\frac{1}{2} W_\vartheta(\bar{\mathbf{e}})^{\frac{1+\vartheta}{2}}, \bar{\mathbf{e}} \in \mathbf{\Xi}_0 \\ \langle dW_\gamma(\bar{\mathbf{e}}) / d\bar{\mathbf{e}}, A\bar{\mathbf{e}} - \mathbf{\Phi}(1, \mathbf{K}, \vartheta, \gamma, \hat{e}_1) \rangle \\ \qquad \leq -\frac{1}{2} W_\gamma(\bar{\mathbf{e}})^{\frac{1+\gamma}{2}}, \bar{\mathbf{e}} \in \mathbf{\Xi}_\infty. \end{cases} \tag{41}$$

The proof process of the two cases is basically the same, thus only $\bar{\mathbf{e}} \in \mathbf{\Xi}_0$ is discussed here. According to Lemma 1, for all $\bar{\mathbf{e}} \in \mathbf{\Xi}_0$, we can obtain

$$\langle dW_\vartheta(\bar{\mathbf{e}}) / d\bar{\mathbf{e}}, A\hat{\mathbf{e}} - \mathbf{\Phi}(1, \mathbf{K}, \vartheta, \gamma, \hat{e}_1) \rangle$$

$$
\begin{aligned}
&= \left\langle \frac{dW_\vartheta(\bar{\mathbf{e}})}{d\bar{\mathbf{e}}}, A\bar{\mathbf{e}} - \boldsymbol{\Phi}'(\mathbf{K},\vartheta,\hat{e}_1) \right\rangle \\
&\quad + \left\langle \frac{dW_\vartheta(\bar{\mathbf{e}})}{d\bar{\mathbf{e}}}, \boldsymbol{\Phi}'(\mathbf{K},\vartheta,\hat{e}_1) - \boldsymbol{\Phi}(1,\mathbf{K},\vartheta,\gamma,\hat{e}_1) \right\rangle \\
&\le -\frac{3}{4} W_\vartheta(\bar{\mathbf{e}})^{\frac{1+\vartheta}{2}} \\
&\quad + \left\langle \frac{dW_\vartheta(\bar{\mathbf{e}})}{d\bar{\mathbf{e}}}, \boldsymbol{\Phi}'(\mathbf{K},\vartheta,\hat{e}_1) - \boldsymbol{\Phi}(1,\mathbf{K},\vartheta,\gamma,\hat{e}_1) \right\rangle .
\end{aligned} \tag{42}
$$

Let us denote $\bar{\mathbf{e}} = \boldsymbol{\Lambda}_\lambda^{\mathbf{r}(\vartheta)} \tilde{\mathbf{z}}$ with $\tilde{\mathbf{z}} \in \boldsymbol{\Xi}$ and $\lambda \in (0,1]$. Then, we obtain

$$
\begin{aligned}
&\langle dW_\vartheta(\bar{\mathbf{e}})/d\bar{\mathbf{e}}, \boldsymbol{\Phi}'(\mathbf{K},\vartheta,\hat{e}_1) - \boldsymbol{\Phi}(1,\mathbf{K},\vartheta,\gamma,\hat{e}_1) \rangle \\
&\quad = 2\lambda^{1+\vartheta} \tilde{\mathbf{z}}^T \mathbf{S} \boldsymbol{\Omega}
\end{aligned} \tag{43}
$$

where $\boldsymbol{\Omega} = [\Omega_1 \quad \Omega_2 \quad \cdots \quad \Omega_n]^T$ for all $1 \le i \le n$, $\Omega_i = k_i[(\mathrm{sgn}^{\vartheta_i}(\lambda\tilde{z}_1) - \varphi(\vartheta_i,\gamma_i,\lambda\tilde{z}_1))/\lambda^{\vartheta_i}] (i = 1,2,\ldots,n)$.

According to Definition 3 and [22, Lemma 4], $\varphi(\vartheta_i,\gamma_i,\lambda\tilde{z}_1)$ uniformly converges to $\mathrm{sgn}^{\vartheta_i}(\lambda\tilde{z}_1)$ on any compact set, when $\vartheta,\gamma \to 1$. Thus, there exists $\varepsilon_1 \in (0,\varepsilon)$ such that

$$
\tilde{\mathbf{z}}^T \mathbf{S} \boldsymbol{\Omega} \le \frac{1}{16} \tag{44}
$$

for every $\vartheta \in (1-\varepsilon_1, 1)$, $\gamma \in (1, 1+\varepsilon_1)$, $\tilde{\mathbf{z}} \in \boldsymbol{\Xi}$, and $\lambda \in (0,1]$.

Finally, we can obtain

$$
\begin{aligned}
&\langle dW_\vartheta(\bar{\mathbf{e}})/d\bar{\mathbf{e}}, A\bar{\mathbf{e}} - \boldsymbol{\Phi}(1,\mathbf{K},\vartheta,\gamma,\hat{e}_1) \rangle \\
&\qquad \le -\frac{3}{4} W_\vartheta(\bar{\mathbf{e}})^{\frac{1+\vartheta}{2}} + \frac{1}{8}\lambda^{1+\vartheta} \\
&\qquad \le -\frac{3}{4} W_\vartheta(\bar{\mathbf{e}})^{\frac{1+\vartheta}{2}} + \frac{1}{8}\left(\lambda^2 W_\vartheta(\tilde{\mathbf{z}})\right)^{\frac{1+\vartheta}{2}} \\
&\qquad \le -\frac{1}{2} W_\vartheta(\bar{\mathbf{e}})^{\frac{1+\vartheta}{2}}
\end{aligned} \tag{45}
$$

for $\forall \bar{\mathbf{e}} \in \boldsymbol{\Xi}_0$ and $\vartheta \in (1-\varepsilon_1, 1)$.

Lemma 3: There exists $M > 0$ such that

$$
\left\langle dW_{\vartheta,\gamma}(\bar{\mathbf{e}})/d\bar{\mathbf{e}}, \Delta_{\omega_0} \mathbf{D} d^{(n-1)} \right\rangle \le M\sqrt{W_{\vartheta,\gamma}(\bar{\mathbf{e}})} \tag{46}
$$

for all $\bar{\mathbf{e}} \in \mathbb{R}^n$, $\vartheta \in (1-\varepsilon_1, 1)$, and $\gamma \in (1, 1+\varepsilon_1)$.

Proof: Inequality (46) is equivalent to

$$
\begin{cases}
\left\langle dW_\vartheta(\bar{\mathbf{e}})/d\bar{\mathbf{e}}, \Delta_{\omega_0} \mathbf{D} d^{(n-1)} \right\rangle \leqslant M\sqrt{W_\vartheta(\bar{\mathbf{e}})}, \bar{\mathbf{e}} \in \boldsymbol{\Xi_0} \\
\left\langle dW_\gamma(\bar{\mathbf{e}})/d\bar{\mathbf{e}}, \Delta_{\omega_0} \mathbf{D} d^{(n-1)} \right\rangle \leqslant M\sqrt{W_\gamma(\bar{\mathbf{e}})}, \bar{\mathbf{e}} \in \boldsymbol{\Xi}_\infty .
\end{cases} \tag{47}
$$

Due to the proof process of the two cases is basically the same, thus, only $\bar{\mathbf{e}} \in \boldsymbol{\Xi}_0$ is discussed here. Define $\bar{\mathbf{e}} = \boldsymbol{\Lambda}_\lambda^{\mathbf{r}(\vartheta)} \tilde{\mathbf{z}}$ with $\tilde{\mathbf{z}} \in \boldsymbol{\Xi}$ and $\lambda \in (0,1]$, one has

$$
\begin{aligned}
&\left\langle dW_\vartheta(\bar{\mathbf{e}})/d\bar{\mathbf{e}}, \Delta_{\omega_0} \mathbf{D} d^{(n-1)} \right\rangle \\
&\quad = \frac{2\lambda^{2-r_n(\vartheta)}}{\omega_0^{n-1}} \tilde{\mathbf{z}}^T \mathbf{S} [0 \quad \cdots \quad 0 \quad d^{(n-1)}]^T .
\end{aligned} \tag{48}
$$

Utilizing Schwartz inequality yields

$$
\left| \tilde{\mathbf{z}}^T \mathbf{S} [0 \quad \cdots \quad 0 \quad d^{(n-1)}]^T \right| \le d_{\max}^{(n-1)} \sqrt{S_{n,n} \tilde{\mathbf{z}}^T \mathbf{S} \tilde{\mathbf{z}}}. \tag{49}
$$

Thus, we can get

$$
\left\langle dW_\vartheta(\bar{\mathbf{e}})/d\bar{\mathbf{e}}, \Delta_{\omega_0} \mathbf{D} d^{(n-1)} \right\rangle \le M\sqrt{W_\vartheta(\bar{\mathbf{e}})} \tag{50}
$$

where $M = 2d_{\max}^{(n-1)} \sqrt{S_{n,n}}/\omega_0^{n-1}$.

REFERENCES

[1] J. Liu, H. Li, and Y. Deng, "Torque ripple minimization of PMSM based on robust ILC via adaptive sliding mode control," *IEEE Trans. Power Electron.*, vol. 33, no. 4, pp. 3655–3671, Apr. 2018.

[2] Z. Sun, Y. Deng, J. Wang, T. Yang, Z. Wei, and H. Cao, "Finite control set model-free predictive current control of PMSM with two voltage vectors based on ultralocal model," *IEEE Trans. Power Electron.*, vol. 38, no. 1, pp. 776–788, Jan. 2023.

[3] H. Cao et al., "Generalized active disturbance rejection with reduced-order vector resonant control for PMSM current disturbances suppression," *IEEE Trans. Power Electron.*, vol. 38, no. 5, pp. 6407–6421, May 2023.

[4] S. Zhu et al., "Robust speed control of electrical drives with reduced ripple using adaptive switching high-order extended state observer," *IEEE Trans. Power Electron*, vol. 37, no. 2, pp. 2009–2020, Feb. 2022.

[5] M. Tian, B. Wang, Y. Yu, Q. Dong, and D. Xu, "Discrete-time repetitive control-based ADRC for current loop disturbances suppression of PMSM drives," *IEEE Trans. Ind. Inform.*, vol. 18, no. 5, pp. 3138–3149, May 2022.

[6] H. Cao et al., "Improved ADRC with a cascade extended state observer based on quasi-generalized integrator for PMSM current disturbances attenuation," *IEEE Trans. Transp. Electrif.*, vol. 10, no. 1, pp. 2145–2157, Mar. 2024.

[7] D. Liang, J. Li, R. Qu, and W. Kong, "Adaptive second-order sliding-mode observer for PMSM sensorless control considering VSI nonlinearity," *IEEE Trans. Power Electron.*, vol. 33, no. 10, pp. 8994–9004, Oct. 2018.

[8] E. Fuentes, C. A. Silva, and R. M. Kennel, "MPC implementation of a quasi-time-optimal speed control for a PMSM drive, with inner modulated-FS-MPC torque control," *IEEE Trans. Ind. Electron.*, vol. 63, no. 6, pp. 3897–3905, Jun. 2016.

[9] Y. Deng, J. Wang, H. Li, J. Liu, and D. Tian, "Adaptive sliding mode current control with sliding mode disturbance observer for PMSM drives," *ISA Trans.*, vol. 88, pp. 113–126, 2019.

[10] T. Yang, et al., "Fast integral terminal sliding mode control with a novel disturbance observer based on iterative learning for speed control of PMSM," *ISA Trans.*, vol. 134, pp. 460–471, 2023.

[11] Ł. J. Niewiara, T. Tarczewski, and L. M. Grzesiak, "Application of extended Kalman filter for estimation of periodic disturbance and velocity ripple reduction in PMSM drive," *Bull. Polish Acad. Sci.. Tech. Sci.*, vol. 68, no. 5, pp. 983–995, 2020.

[12] Ł. J. Niewiara, T. Tarczewski, and L. M. Grzesiak, "Application of state feedback controller with feedforward for velocity ripples reduction of PMSM drive at low speed operation," in *Proc. 21st Eur. Conf. Power Electron. Appl.*, 2019, pp. P.1–P.10.

[13] S. You, J. Gil, and W. Kim, "Adaptive neural network control using nonlinear information gain for permanent magnet synchronous motors," *IEEE Trans. Cybern.*, vol. 53, no. 3, pp. 1392–1404, Mar. 2023.

[14] J. Han, "From PID to active disturbance rejection control," *IEEE Trans. Ind. Electron.*, vol. 56, no. 3, pp. 900–906, Mar. 2009.

[15] B. Guo, S. Bacha, M. Alamir, A. Hably, and C. Boudinet, "Generalized integrator-extended state observer with applications to grid-connected converters in the presence of disturbances," *IEEE Trans. Control Syst. Technol.*, vol. 29, no. 2, pp. 744–755, Mar. 2021.

[16] H. Sira-Ramirez and M. A. Oliver-Salazar, "On the robust control of buck converter DC-motor combinations," *IEEE Trans. Power Electron.*, vol. 28, no. 8, pp. 3912–3922, Aug. 2013.

[17] V. Andrieu, L. Praly, and A. Astolfi, "Homogeneous approximation, recursive observer design, and output feedback," *SIAM J. Control Optim.*, vol. 47, no. 4, pp. 1814–1850, Jan. 2008.

[18] A. Polyakov, "Nonlinear feedback design for fixed-time stabilization of linear control systems," *IEEE Trans. Autom. Control*, vol. 57, no. 8, pp. 2106–2110, Aug. 2012.

[19] B. Jiang, Q. Hu, and M. I. Friswell, "Fixed-time attitude control for rigid spacecraft with actuator saturation and faults," *IEEE Trans. Control Syst. Technol.*, vol. 24, no. 5, pp. 1892–1898, Sep. 2016.
[20] S. Chang, Y. Wang, and Z. Zuo, "Fixed-time active disturbance rejection control and its application to wheeled mobile robots," *IEEE Trans. Syst. Man Cybern. Syst.*, vol. 51, no. 11, pp. 7120–7130, Nov. 2021.
[21] J. Ni, Y. Tang, and P. Shi, "A new fixed-time consensus tracking approach for second-order multiagent systems under directed communication topology," *IEEE Trans. Syst. Man Cybern. Syst.*, vol. 51, no. 4, pp. 2488–2500, Apr. 2021.
[22] T. Menard, E. Moulay, and W. Perruquetti, "Fixed-time observer with simple gains for uncertain systems," *Automatica*, vol. 81, pp. 438–446, 2017.
[23] M. Piao, Y. Wang, M. Sun, X. Zhang, Z. Chen, and Y. Yan, "Fixed-time-convergent generalized extended state observer based motor control subject to multiple disturbances," *IEEE Trans. Ind. Inform.*, vol. 17, no. 12, pp. 8066–8079, Dec. 2021.
[24] Z. Hao et al., "Linear/nonlinear active disturbance rejection switching control for permanent magnet synchronous motors," *IEEE Trans. Power Electron.*, vol. 36, no. 8, pp. 9334–9347, Aug. 2021.
[25] J. Li, Y. Xia, X. Qi, and Z. Gao, "On the necessity, scheme, and basis of the linear-nonlinear switching in active disturbance rejection control," *IEEE Trans. Ind. Electron.*, vol. 64, no. 2, pp. 1425–1435, Feb. 2017.
[26] P. Lin, Z. Wu, K.-Z. Liu, and X.-M. Sun, "A class of linear/nonlinear switching active disturbance rejection speed and current controllers for PMSM," *IEEE Trans. Power Electron.*, vol. 36, no. 12, pp. 14366–14382, Dec. 2021.
[27] W. Qian, S. K. Panda, and J.-X. Xu, "Torque ripple minimization in PM synchronous motors using iterative learning control," *IEEE Trans. Power Electron.*, vol. 19, no. 2, pp. 272–279, Mar. 2004.
[28] A. H. M. Sayem, Z. Cao, and Z. Man, "Model free ESO-based repetitive control for rejecting periodic and aperiodic disturbances," *IEEE Trans. Ind. Electron.*, vol. 64, no. 4, pp. 3433–3441, Apr. 2017.
[29] B. Wang, M. Tian, Y. Yu, Q. Dong, and D. Xu, "Enhanced ADRC with quasi-resonant control for PMSM speed regulation considering aperiodic and periodic disturbances," *IEEE Trans. Transp. Electrif.*, vol. 8, no. 3, pp. 3568–3577, Sep. 2022.
[30] M. Tian, B. Wang, Y. Yu, Q. Dong, and D. Xu, "Adaptive active disturbance rejection control for uncertain current ripples suppression of PMSM drives," *IEEE Trans. Ind. Electron.*, vol. 71, no. 3, pp. 2320–2331, Mar. 2024.
[31] C. Xia, B. Ji, and Y. Yan, "Smooth speed control for low-speed high-torque permanent-magnet synchronous motor using proportional-integral-resonant controller," *IEEE Trans. Ind. Electron.*, vol. 62, no. 4, pp. 2123–2134, Apr. 2015.
[32] J. P. Gauthier, H. Hammouri, and S. Othman, "A simple observer for nonlinear systems applications to bioreactors," *IEEE Trans. Autom. Control*, vol. 37, no. 6, pp. 875–880, Jun. 1992.
[33] A. A. Godbole, J. P. Kolhe, and S. E. Talole, "Performance analysis of generalized extended state observer in tackling sinusoidal disturbances," *IEEE Trans. Control Syst. Technol.*, vol. 21, no. 6, pp. 2212–2223, Nov. 2013.
[34] Q. Hou, Y. Zuo, J. Sun, C. H. T. Lee, Y. Wang, and S. Ding, "Modified nonlinear active disturbance rejection control for PMSM speed regulation with frequency domain analysis," *IEEE Trans. Power Electron.*, vol. 38, no. 7, pp. 8126–8134, Jul. 2023.

Xiufeng Liu (Graduate Student Member, IEEE) was born in Changchun, China, in 1998. He received the B.E. degree in vehicle engineering from Changchun University of Technology, Changchun, China, in 2020. He is currently working toward the Ph.D. degree in mechatronic engineering with the University of Chinese Academy of Sciences, Beijing, China, and the Changchun Institute of Optics, Fine Mechanics and Physics, Chinese Academy of Sciences, Changchun, China.

His main research interests include advanced control theories and applications on motor drive systems.

Yongting Deng (Senior Member, IEEE) was born in Shandong, China, in 1987. He received the B.E. degree in automation from the China University of Petroleum (East China), Qingdao, China, in 2010, and the M.S. degree in mechatronic engineering and the Ph.D. degree in mechatronic engineering from the Changchun Institute of Optics, Fine Mechanics and Physics, Chinese Academy of Sciences, Changchun, China, in 2015.

He is currently a Professor with the Changchun Institute of Optics, Fine Mechanics and Physics, Chinese Academy of Sciences. He has authored or coauthored more than 70 publications in the research interests that include controller design for ac motor drives and linear motor drives, intelligent control, and high-precision machine control techniques.

Jianli Wang (Member, IEEE) was born in Shandong, China, in 1971. He received the Ph.D. degree in mechatronic engineering from the Changchun Institute of Optics, Fine Mechanics and Physics, Chinese Academy of Sciences, Changchun, China, in 2002.

He is currently a Professor with the Changchun Institute of Optics, Fine Mechanics and Physics, Chinese Academy of Sciences. He has authored or coauthored more than 100 publications in his main areas of research, which are optical-electric telescope, high-resolution imaging, and high-precision machine control techniques.

Hongwen Li (Member, IEEE) was born in Sichuan, China, in 1970. He received the M.S. degree in control theory and control engineering from the Jilin University of Technology, Changchun, China, in 1996, and the Ph.D. degree in control theory and control engineering from Jilin University, Changchun, China, in 2007.

From 1996 to 2002, he was an Associate Professor with the Jilin University of Technology. Since 2002, he has been with the Changchun Institute of Optics, Fine Mechanics, and Physics, Chinese Academy of Sciences, Changchun, where he is currently a Professor with the Department of Optical-Electronic Detection. He has authored/coauthored more than 50 publications in these areas. His research interests include optical-electric sensor technologies, switching-mode power supply techniques, electric machines and drives, and high-precision machine control techniques.

Haiyang Cao (Graduate Student Member, IEEE) was born in Shangdong, China, in 1997. He is currently working toward the Ph.D. degree in mechatronic engineering with the University of Chinese Academy of Sciences, Beijing, China, and the Changchun Institute of Optics, Fine Mechanics and Physics, Chinese Academy of Sciences, Changchun, China.

Since October 2023, he has been a joint Ph.D. student with Nanyang Technological University, Singapore. His main research interests include advanced control theories and applications on motor drive systems.